Macromolecular Engineering towards the Fabrication of Biomimetic Membranes with Water Channel Proteins for Desalination Applications

by

Yuan He

A thesis submitted in partial fulfillment of the requirements for the degree of

Master of Science

in
Materials Engineering

Department of Chemical and Materials Engineering
University of Alberta

Abstract

Due to the fast development of human society and high growth of world population, fresh water shortage has become one of the most critical and urgent problems of our society. Since the discovery of aquaporins (water channel proteins), researchers have been trying to incorporate them as functional units in biomimetic material to achieve superior water permeability and solute rejection. Although the biomimetic desalination membrane technology with aquaporins has gained growing interest, it is still challenging to effectively stabilize aquaporins and fabricate robust membranes with high water permeability and salt rejection. In this work, amphiphilic peptides (BP-1 and FBP-1) were applied to stabilize aquaporin (AqpZ). From there, two novel strategies were devised to prepare AqpZ-containing membranes for desalination purpose. In the first design, AqpZ/BP-1 complex was prepared and successfully encapsulated into a dense polyamide barrier layer via interfacial polymerization on a polysulfone substrate. The resulting composite membrane showed enhancement of water permeability (28% improvement compare to negative control membrane) while maintaining high salt rejection (96%) over the testing time. In the second design, AqpZ/FBP-1 complex with alkynyl group was synthesized and then conjugated with azide functionalized porous polymeric substrate. Surface morphology imaging and surface chemical composition analyses suggest successful conjugation between the complex and the surface. The consequent membrane displays enhanced salt rejection. Both strategies showed great potential of incorporating AqpZ into membrane system for desalination applications.

Acknowledgements

I would like to express my sincere gratitude to my supervisor Dr. Carlo Montemagno, who recruited me and offered me the opportunity to learn to be a researcher in the Ingenuity Lab, working alongside other amazing researchers. I sincerely appreciate his valuable advice and guidance in my work. His creativity and enthusiasm for research, the way he organized Ingenuity Lab, his wonderful communication skills and optimistic attitude all show me how a great researcher could be.

I am also very grateful to Dr. Sinoj Abraham. He has rich experience in polymer synthesis and he helped me a great deal with experimental design. His creative thoughts and insightful ideas helped broaden my vision of my research. In addition, I would like to thank Dr. Hiofan Hoi. Her rich knowledge in biology, her critical thinking and her precise and rigorous attitude to academic research inspired me. Meanwhile, as my friend, her encouragement and support motivated me to move forward during my master study.

Many thanks to Ms. Sumalee Salahub, Mr. Antonio Jiménez, Dr. Surjith Kumaran, Dr. Guibin Ma, Ms. Jeanine Koshelek, Ms. Hang Zhou and all my other group mates for their support in my research. I would also like to acknowledge Peng Li from Nanofab and Hui Qian from National Institute for Nanotechnology (NINT), for the materials characterizations and technical support.

Last but not least, I would like to thank my parents and my friends for their consistent support and encouragement on my studies and my life in Canada.

Table of contents:

List of Tables:

List of Figures:

Chapter 1 Introduction

Water is one of the essential sources for human life on earth. Water not only supports the basic living function of human being, but also has significant influence on the whole living society including energy and food production, industrial output, and the quality of our environment. Therefore, a clean and adequate water supply is required in order to develop our society[1]. However, the fresh water from nature is not adequate as commonly assumed. Although 71% of the earth surface is covered by water, 96.5% of earth water is hold by oceans，which is not able to be directly used due to its high salinity. Only 0.3% of earth water is regarded as accessible fresh water, while the remaining fresh water is located deep underground or solidified as ice or snow and regarded as unavailable[2]. Meanwhile, due to the rapid growth of world population, water shortage becomes worse. Over 17% of population are without clean drinking water and approximately 41% of population live in water shortage regions[3]. In addition, as fast development in industry and contamination of freshwater resources, the global freshwater supply has kept rapidly depleting.

Water reuse and desalination of salt water have become two main methods to increase fresh water supply from available source[1]. Water reuse has been used as a method for indirect drinking water production[4], while desalination, a process that converts salt water into clean water, has become a significant solution for drinking water production[5]. Driven by the demand for adequate fresh potable water, a reliable, effective and energy efficient water desalination system is urgently need.

1.1 Current desalination technologies and their limitations

Generally, there are two major types of water desalination techniques: i) phase-change/ thermal techniques, including multi-effect distillation (MED) and multi-stage flash (MSF); ii) membrane based technology, which is widely known as reverse osmosis (RO)[6].

For thermal techniques, MED is the oldest desalination process[7] and it is based on heat transport from condensing steam of salt solution in a series of stages. In each stage, the feed water is heated and partly evaporated by steam in the tubes, generating secondary water steam for next stage. Meanwhile the steam is condensed and collected as fresh water[7]. Although the MED process achieves high heat transfer rates[8], disadvantages of corrosion and scaling of oversaturated compounds like $CuSO_4$ become a major concern[9]. MSF came into practice in the 1960s because of the ease and reliability of the process[10]. During MSF process, vapor is generated from feed water when it enters into an evacuated chamber. The process is repeated at each stage with successively decreasing pressure. The vapor is subsequently condensed and fresh water is obtained[10]. For MSF, corrosion is easier to control compared to MED, however, it has lower performance ratio, which results in higher energy consumption. Moreover, both MED and MSF processes require an external steam supply, which makes them expensive technologies and not the best economical choice for the whole society.

RO first appeared in the early 1950s[11] and became competitive with classical thermal techniques in the 1980s due to the materials development and technique improvement. It uses a semipermeable membrane to remove solutes from feed solution under certain pressure. Compared with MED and MSF, RO process has advantages including high efficiency, no corrosion and no heat energy consumption. This suggests that the RO process has lower cost in

producing water, which could be as low as around 0.5-0.7 US$/m^3, one-half to one-third of the cost of MSF and MED[12, 13]. Therefore, in terms of process flow and energy consumption, RO becomes the leading and promising desalination technology to overtake the classical thermal technologies[14].

However, making RO desalination plants affordable in poorer countries still remains challenging in practice[15]. Therefore, technology developments to further reduce the costs of RO plants are necessary. As RO cost is mostly attributed to energy, labor and chemicals, new inventions in membrane material and membrane structure design can significantly help in reducing from all three aspects of RO cost[15]. Advanced RO membranes with higher water permeability and salt rejection result in higher efficiency system and lower operating pressure, which leads to considerable reduction in energy consumption. Meanwhile, increased efficiency of RO system results in reduction in membrane area. As a consequence, less membrane is required, leading to further reduction in membrane replacement costs, smaller plant footprint and reduced use of chemicals[15]. Therefore, novel ultrahigh permeability membrane system without sacrificing salt rejection performance is a promising solution to the fresh water shortage challenge.

1.2 Reverse osmotic membrane technology and technical challenges

As shown in Figure 1.1, during the RO process, an external pressure is applied to overcome osmotic pressure. Consequently, water molecules are forced to pass through the semi-permeable membrane, while salt ions are rejected by the membrane, which leads to salt removal from feed water[16]. As a result, novel materials and designs for highly selective RO membranes have

become the core factors to enhance the efficiency of RO process.

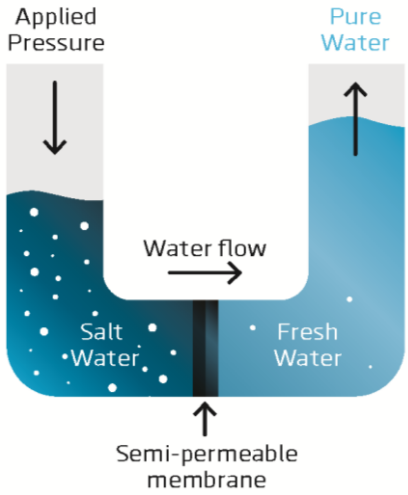

Figure 1.1 Diagram of RO process. The semi-permeable membrane in the middle separates the two regions of salt water (left side) and fresh pure water (right side). The white dots represent salt ions in the solution.

Conventional RO membranes are mostly made up by polymer materials due to their low-cost fabrication, robust mechanical property and improved performance in selectivity and permeability. In the late 1950's, Reid et al.[17] first reported that a thin symmetrical cellulose acetate (CA) membrane had the capability to reject salt passage from salted water. However, the water flux obtained was too small and uneconomical to be practical. Then, in the early 1960's, Loeb et al.[18] developed a simple asymmetric CA membranes with the structure of a dense thin skin layer over a thick micro-porous sublayer, using a phase inversion membrane fabrication technique. This membrane showed relatively high water flux and salt rejection, making RO process both possible and practical. Since then, cellulose derivatives have been studied as the materials to fabricate RO membranes. Joshi et al.[19] investigated cellulose triacetate (CTA) to

cast RO membranes due to its better stability and easiness to fabricate compared to initial CA. High salt rejection was achieved from this membrane. However, CTA membrane has the trend of compaction, resulting in severe flux drop during the test. Moreover, the hydrolysis of acetate group in CA materials and weak resistance to contamination became the major drawbacks of CA membranes[20]. Therefore, new materials with better chemical stability for casting RO membrane were required. Several non-cellulosic asymmetric membranes with similar structures of a very thin skin layer supported on a more porous sublayer of the same material were developed by using aromatic polyamide[21], polypiperazine-amides[22], polybenzimidazoline[23], and etc.. Although they showed higher stability compared to CA membranes, the salt rejection and water permeability were relatively lower. However, only a few polymers were qualified for the casting procedure of asymmetric membranes and even less consequent membranes showed attractive water permeability and salt rejection property. In addition, the asymmetric structure hindered and slowed down water molecules movements as the densification occurred in the middle layer of the membrane[15].

The limitations of asymmetric membranes led to inventions of composite membranes. Typical composite membranes usually consist of a porous substrate for mechanical support and a thin barrier layer for salt rejection. Given by the composite structure, the two parts were able to be optimized separately, and more polymers and polymerization processes can be tested for barrier layer or substrate[15]. For the substrate, polysulfone was found to be the optimum material because of its high mechanical resistance to compaction and chemical stability[24]. For the barrier layer, polyamide was developed as the main material for the ultra-thin layer on top of the porous substrate. To enhance the desalination performance, the barrier layer should be

ultra-thin while dense enough to prevent ion leakage. Cadotte et al.[25] first used polyethylenimine and toluene di-isocyanate to develop the barrier layer by interfacial polycondensation and fabricated a RO membrane named NS-100. This was a major technological milestone in RO history as it was the first successful non-cellulose membrane with comparable water desalination performance. Since then, different amine such as polypyrolidine[26] and piperazine[27], and different acyl chloride like trimesoyl chloride were tested as the monomers for interfacial polycondensation. In 1981, Cadotte et al.[28] found that membranes fabricated by monomeric aromatic amines and aromatic acyl chloride achieved best results of desalination performance among others. Moreover, the membrane provided a high mechanical, thermal and chemical resistance. This revolutionary success shifted the research and developments focus from materials development to the optimization of interfacial reaction condition. Certain achievements in this aspect have been reported [29]. However, the improvements of membrane desalination performance has been limited since the late 1990s[15]. Therefore, new concept and new model of membrane should be built to further improve the desalination performance of RO membranes.

1.3 Biomimetic desalination membranes

1.3.1 Aquaporins

In nature, the challenge of having a highly efficient and pure water exclusively permeable system has already been solved. Cell membranes are considered as ideal solute rejecting desalination biological membranes. Across a cell membrane, a composite set of membrane transport proteins have taken charge of the movements of specific ions, small molecules and

organic macromolecules. The enhanced permeability and high selectivity to water molecule is due to the presence of water channel proteins, aquaporins (AQPs) [30].

The mechanism of water transports through AQPs is channel-mediated transportation due to its featured structure. The walls of AQPs channel are consisted of six transmembrane helices. The center of the channel is made up by two Asparagine–proline–alanine (NPA) motifs[31], which form a 3D "hourglass" structural filter for water molecules to flow through (Figure 1.2)[32]. The other filter is called the aromatic/arginine (ar/R) selectivity filter, which forms the narrowest part of the channel. It is made up by a cluster of amino acids to help orient and bind with water molecules. When water molecules are passing the selectivity filter, water–water hydrogen bonds are replaced by water-protein interaction. In the same time other molecules such proton, ions and organic molecules are prevented from entering the channel by steric exclusion and electrostatic repulsion[31]. Given by the unique structure, AQPs has a ultra-high transport rate of water molecules, which reaches approximately 3×10^9 water molecules per subunit per second[33]. Therefore, Incorporating AQPs into membrane technology system becomes a promising strategy for building highly efficient desalination plants.

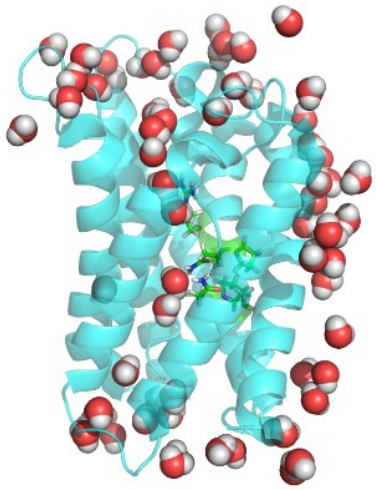

Figure 1.2 Schematic representation of water molecules passing through the channel of AQPs

1.3.2 AQPs stabilizing methods

Due to the relatively hydrophobic property of membrane proteins, stabilizing agents are required to prevent protein aggregation after proteins are purified from the cell membranes. For biomimetic desalination membranes fabrication, tight and organized stabilizing structure for AQPs is demanded in order to be compatible with the designed system while maintaining AQPs' functionality.

As AQPs are stabilized by the lipid bilayer in their native environment, synthetic or purified lipids that can form bilayers are suitable candidates to stabilize AQPs *in vitro*. The lipid bilayer is consisted of two opposed layers of amphiphilic lipid molecules. They have a specific chemical structure with a polar head group and two nonpolar hydrocarbon tails (Figure 1.3a). Due to the cylindrical shape and amphiphilic nature, they tend to self-assemble into bilayers with polar head groups directly toward aqueous phase and nonpolar tails sequestered in the interior of the two layers with each other. As the compatible hydrophobicity between the interior of bilayer and exterior of AQPs, lipid bilayer structure is capable to reconstitute membrane proteins by hydrophobic force, forming a stable and functional integral unit for downstream applications. Moreover, lipid bilayers tend to fold themselves into sealed structures such as liposomes (Figure 1.3b), as it minimizes the nonfavorable contact between water molecules and nonpolar tails at the free edge area[34]. The resulting liposomes with AQPs incorporated in are known as proteoliposomes. So far, the most widely used lipid stabilizing agents for AQPs in membrane fabrication include 1,2-dioleoyl-sn-glycero-3-phosphocholine (DOPC), which is extracted

directly from *Escherichia coli (E. coli)* [35], 1,2-diphytanoyl-sn-glycero-3-phosphocholine (DPhPC), 1,2-dioleoyl-sn-glycero-3-phospho-(1′-rac-glycerol) (sodium salt) (DOPG), and 1,2-dioleoyl-3-trimethylammonium-propane (chloride salt) (DOTAP)[36].

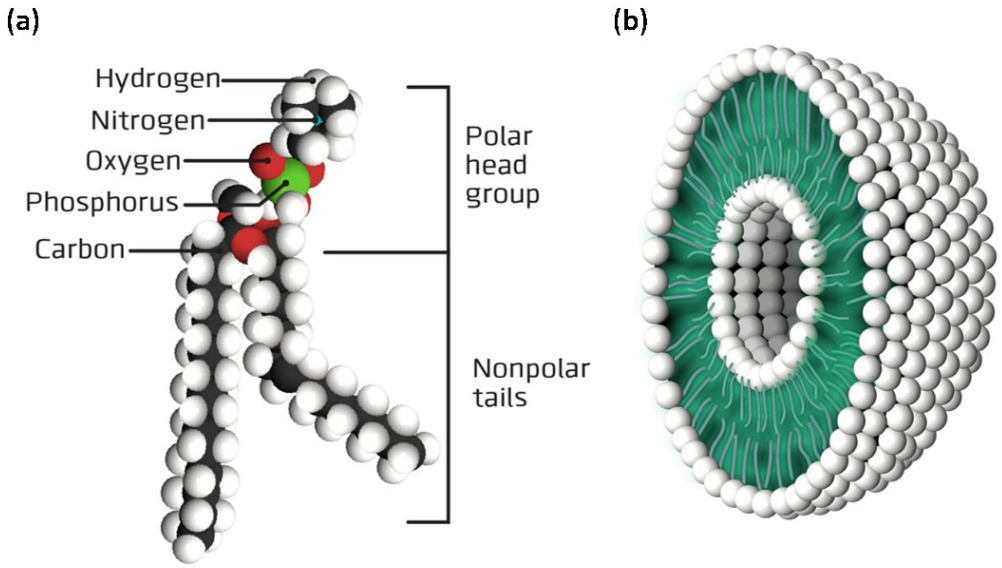

Figure 1.3(a) Symbol structure of the lipid from lipid bilayers. Different color represents different elements; (b) Schematic drawing of three-dimensional view of a liposome structure formed by lipids.

However, lipids are usually sensitive to the environmental factors such as pH, temperature, ionic strength, etc., which leads to the poor stability of liposomes as hydrolytic and oxidative decomposition may occur[37]. Hence, synthetic amphiphilic block copolymers, made up by blocks of different hydrophobicity monomers, become promising alternative materials due to superior chemical and mechanical stability[38]. As shown in Figure 1.4a, similar to the lipids, amphiphilic block copolymers can assemble into polymersomes with bilayer-like structure in

aqueous phase[39, 40]. Stoenescu et al. [41] first incorporated AQPs into polymersomes made of triblock polymer (e.g. ABA, ABC, CBA, where A stands for poly-2-methyloxazoline (PMOXA), B for polydimethylsiloxane (PDMS) and C for polyethylene oxide (PEO)). Kumar et al.[42] incorporated a bacterial aquaporin, Aquaporin Z (AqpZ) into PMOXA-PDMS-PMOXA polymersomes (structure as shown in Figure 1.4b) and first demonstrated the functionality of AqpZ in the polymersome. The huge increase in permeability indicates the potential of amphiphilic block copolymers as a superb alternative to incorporate AQPs into system for further applications.

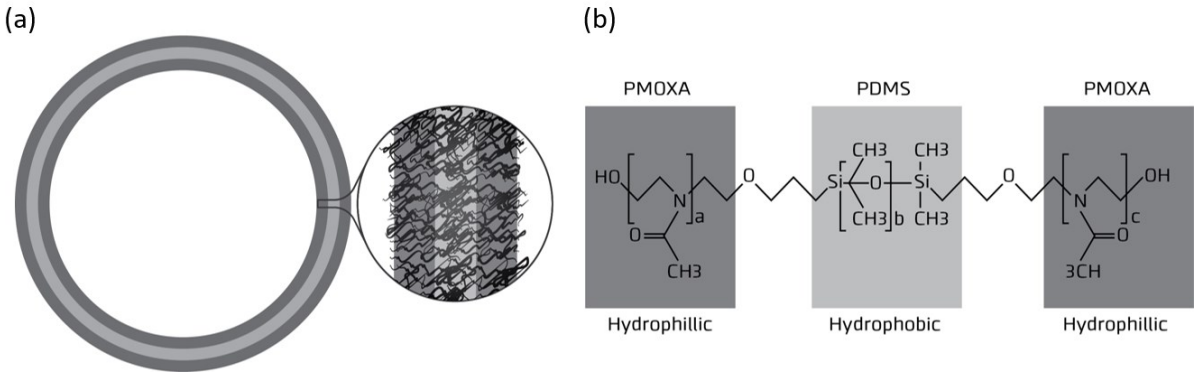

Figure 1.4(a) Schematic representation of the cross section of block copolymer vesicle; (b) The chemical structure of PMOXA-PDMS-PMOXA triblock polymer. The dark grey areas indicate the hydrophilic PMOXA segments and the light grey area shows the hydrophobic PDMS segments in polymer chain.

Recently, Tao et al.[43] invented a new method to stabilize membrane proteins. They demonstrated that short amphiphilic β-strand peptides can be a universal reagent to improve the stability of membrane proteins and facilitate general applications[43]. Four types of membrane proteins were successfully stabilized by the β-strand peptides including alpha helix membrane

proteins which have similar secondary structure as AQPs. For the structure of the peptide, the following requirements should be achieved: 1) alternating sequence periodicity of polar and nonpolar amino acids residues in the peptide to control the formation of β-strand [44]; 2) short amino acid sequence with a length comparable to the nonpolar part of membrane bilayers [45]; 3) elongated alkyl side chains at each end of the peptide to mimic lipid bilayers [46]; 4) Modifying amino acid with N-methyl group to increase its water solubility[47]. The general sequence they developed of the designed β-strand peptides is acetyl-(octyl)Gly-Ser-Leu-Ser-Leu-Asp-(octyl)Gly-Asp-NH_2 (BP-1), as shown in Figure 1.5a. The authors reasoned that the β-strand peptides are able to span and cover the hydrophobic surfaces of membrane proteins by forming an ordered and stabilized secondary β-barrel structure around the protein. Moreover, they claimed that the β-strand peptides tightly bound with each other through intermolecular hydrogen-bonding and thus have a lower tendency to dissociate from protein surfaces (Figure 1.5b). Therefore, the β-strand peptides provide a new method to better stabilize membrane proteins without constraining protein functionality for subsequent applications[43].

In this thesis, a procedure to prepare AqpZ stabilized with BP-1 was developed and the structure of the AqpZ/BP-1 complex was characterized. Subsequently, AqpZ/BP-1 complex was incorporated into desalination membrane system to enhance the water permeability of the membrane, while maintaining its high salt rejection.

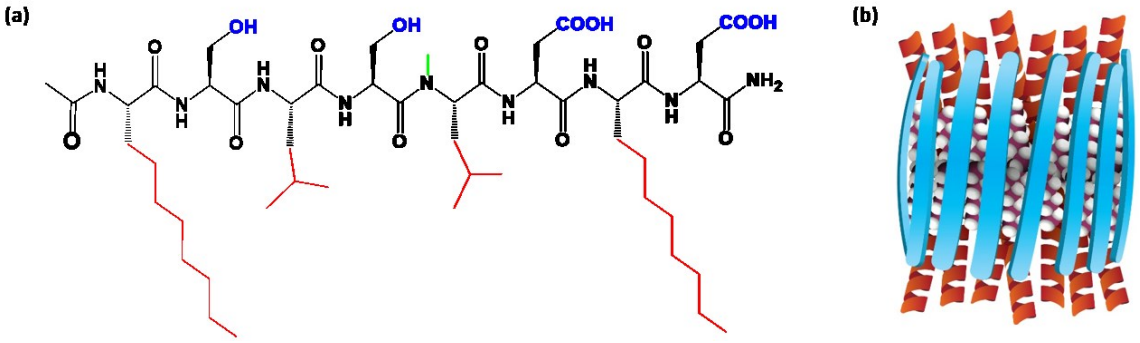

Figure 1.5(a) The sequence of BP-1 with alternate nonpolar (red) and polar (blue) residues, and one N-methyl modified amino acid in the middle (green); (b) Cartoon representation of β-barrel architecture assembled from β-strand peptides (blue strands) in which the hydrophobic alkyl chains (white spheres) bound with the membrane protein surfaces (red alpha-helices)

1.3.3 Recent research on AQPs embedded biomimetic membranes

Given to the supreme water permeability and solute rejection of AQPs, robust AQP incorporated membranes are potential candidates for practical desalination application. Ideal AQPs embedded biomimetic membranes should have the following properties:1) high permeability and salt rejection; 2) mechanical robustness for required pressure as a reverse osmosis membrane; 3) chemical and biological stability for long term use, and 4) easy to scale up. For fabricating the membranes, it is crucial to effectively load AQPs onto support membranes meanwhile maintaining the protein function. The integration of AQPs amphiphilic units (as mentioned above) with an appropriated substrate is a crucial step to design a successful biomimetic membrane for desalination. Two main strategies have been reported so far.

One strategy is to fabricate a single thin layer of lipid bilayer or amphiphilic block copolymer layer incorporated with AQPs on the surface of porous support (Figure 1.6a). Usually it contains two steps: 1) AQPs were stabilized and incorporated into vesicles made by liposomes

or polymersomes; 2) Vesicles were then ruptured and extended on the appropriate porous surface to form an ultra-thin layer with AQPs. Li et al.[48] first spin-coated a layer of positively charged lipids on a nanofiltration substrate and then fused AQPs proteoliposomes onto the modified substrate to fabricate the biomimetic membrane. Wang et al. [49] fused AQPs proteoliposomes onto two different substrates, a simple porous alumina substrate and a gold-coated porous alumina which was further modified by carboxylated polyethylene glycol (PEG) cushion. The carboxylated-PEG cushion significantly enhanced the flexibility, which led to improved mechanical strength of the membrane. Due to the electrical properties of phospholipids and polyelectrolytes, a layer by layer (LbL) assembly strategy was applied to construct composite membranes by electrostatic attraction between the oppositely charged proteoliposomes and polyelectrolytes substrates. Wang et al.[50] deposited AQPs incorporated vesicles with positive charges on an LbL complex polyelectrolyte membrane with negative charges to fabricate a biomimetic nanofiltration membrane. The membrane exhibited high mechanical stability and less defects and was able to maintain good water permeability and salt rejection.

Other than lipid vesicles, amphiphilic block copolymers are excellent alternative reconstitution agents for incorporating AQPs into membranes, due to their relatively higher stability. Wang et al.[51] incorporated AQPs into the PMOXA-PDMS-PMOXA (ABA) polymersomes via typical proteopolymersomes synthesis. A porous polycarbonate tracked-etched (PCTE) substrates was modified with photo-reactive acrylate functional groups on the top. The proteopolymersomes were subsequently deformed to cover the pores of the substrate under an applied pressure. Meanwhile, a covalent bond between the ABA polymer and the substrate was formed by UV polymerization, resulting in vesicle fusion. Duong et al.[52]

ruptured disulfide-functionalized ABA triblock copolymer proteopolymersomes onto gold coated porous alumina membranes. Different pore size of alumina substrates were investigated for vesicles spreading. Zhong et al.[53] deformed methacrylate functionalized ABA copolymer proteopolymersomes on modified cellulose acetate membrane. The membrane was subsequently polymerized by UV. The membrane exhibited impressive water permeability as a loose RO membrane.

In conclusion, the single thin layer strategy has advantages of good biocompatibility and fast transportation of water molecules, as the barrier layer is just several nanometers thick. However, low mechanical stability and relatively low salt rejection due to defect formation are the main inherent drawbacks for large-scale practice.

In order to enhance the mechanical stability and reduce defect formation of the biomimetic membrane, another strategy was developed by encapsulating AQPs vesicles into a dense polymer layer on a porous support while remaining the vesicle sphere structure (Figure 1.6b). Zhao et al.[54] synthesized a robust membrane by embedding AQPs proteoliposomes into a thin film composite (TFC) barrier by interfacial polymerization. That was the first study reporting the preparation of AQPs embedded biomimetic membranes using the interfacial polymerization method. The resulting membrane showed superior separation performance and good mechanical stability under high testing pressure. Li et al.[55] decorated AQPs proteoliposomes with polydopamine (PDA) to increase their affinity to the membrane substrate. Subsequently, the proteoliposomes were immobilized on a polyaminde-imide substrate. Then a selective layer was fabricated by crosslinking polyelectrolyte with the substrate to encapsulate the proteoliposomes. Their work also revealed that AQPs molecules are relatively thermostable as they maintained a

relatively high activity after incubation at 343 K for 2 h. Sun et al.[56] first prepared amine-functionalized PEGylated AQPs proteoliposomes, and then stabilized them by using UV polymerization method to crosslinking the polymers inside the lipid bilayer. These proteoliposomes were subsequently immobilized on a PDA coated porous membrane via a pressure-assisted adsorption method. The membrane was further cross-linked with glutaraldehyde to improve the proteoliposomes stability on the membrane surface. Sun et al.[57] introduced poly-L-lysine (PLL) decorated proteoliposomes into an LbL cationic polyelectrolyte/anionic polyelectrolyte membrane. The LbL technique facilitated the formation of a well-ordered selective layer with proteoliposomes by electrostatic interactions. To further encapsulated proteoliposomes into membrane dense layer, Sun et al. [58] developed a magnetic-aided LbL method. Proteoliposomes containing magnetic nanoparticles were synthesized and subsequently encapsulated into a multilayer polyelectrolyte membrane with the assistance of applied magnetic field. More proteoliposomes were able to be deposited to enrich the loading efficiency of AQP in biomimetic membrane.

Besides liposomes, polymersomes are common candidates for reconstituting AQPs into the dense layer of the membrane, due to their higher mechanical stability and ability to prevent vesicles from deforming under testing pressure. Wang et al. [59]reconstituted AQPs into UV cross-linkable polymersomes with disulfide anchors. The vesicles were partially intruded into the pore by a critical pressure and covalently conjugated to gold coated surface. Subsequently the proteopolymersomes were covered by a dense selective layer of PDA-histidine. This design effectively prevented proteopolymersomes from being peeled off during desalination process. Xie et al.[60] designed a novel “Aquaporin vesicle-imprinted membrane”. Similarly, AQPs were

incorporated in cross-linkable hydroxyl functionalized polymersomes. After conjugating the cross-linked proteopolymersomes onto the amine functionalized CA substrate by amidation reaction, *in situ* surface imprinting polymerization was conducted to generate a nano-sized uniform dense hydrophobic polymer layer to encapsulate the vesicles.

Compared with the single thin layer strategy, encapsulating AQPs vesicles into dense polymer layer gave advantages of mechanically robustness, higher protection for AQPs from polymer matrix and easy to scale up. Nevertheless, further research should be directed toward AQPs incorporation limit in vesicles, vesicles packing density and ionic leakage in biomimetic membranes[37].

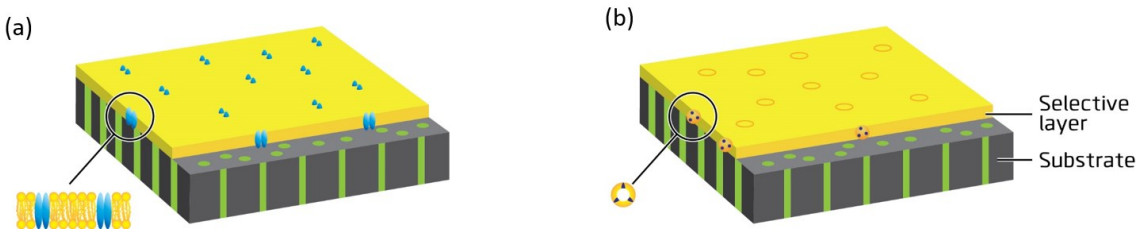

Figure 1.6 Schematic diagram of AQPs biomimetic membranes: (a) AQPs (blue) is embedded in a single flat bilayer (yellow) deposited on a porous support (gray); and (b) AQP vesicles (orange) are encapsulated in a dense polymer layer (yellow) on a porous support substrate (gray).

In fact, the desalination performance of most biomimetic membranes mentioned above were not characterized, or the salt rejection was found out to be too low to consider them as RO membranes, due to their fragile structures and defects in membrane formation. Therefore, new membrane designs should be developed to efficiently incorporate active AQPs into the membrane system while enhance membrane mechanical stability and environmental tolerance.

1.4 Scope of work

In this work, I present a novel method to stabilize AQPs and come up with two incorporation and fabrication strategies. Inspired by Tao and co-workers work on β-strand peptides[43], rather than lipids or block copolymers, I utilized the short amphiphilic peptide to protect and improve the stability of AQPs in the membrane. This amphiphilic peptide has a sequence of alternating polar and nonpolar residues to form β-sheet in solution, and in the presence of protein it wraps around the protein to form a AQP/peptide complex. I then encapsulated AQP/peptide complex into a thin film composite polyamide barrier layer by interfacial polymerization to form a robust and defect-free biomimetic RO membrane[54].

I also attempted to covalently immobilize AqpZ/peptide complex on substrate to achieve better control on the protein assembly. Click chemistry was chosen as the conjugation chemistry given its high selectivity and bio-compatibility[61]. A functional amino acid with alkynyl group was added into the amphiphilic peptide sequence, yielding a functionalized peptide that has capabilities of conjugating to substrate and stabilizing AQP. For the substrate, I first modified polysulfone with azide group, then casted the membrane using a liquid-induced phase inversion technique, resulting in functional substrate with pore size suitable for AQP/peptide complex loading. Subsequently, the click reaction was conducted under circulating condition using a peristaltic pump. The azide functionality and the circulate reaction provide the provision for specific attachment of functional complex. Thus, the AQP/peptide complex can be covalently crosslinked to the substrate through mild click chemistry, resulting in a robust protein-loaded biomimetic membrane.

Objectives of this thesis include:

- To confirm that β-sheet peptide and functionalized β-sheet peptide can stabilize AqpZ, which is the water channel protein from *E. coli*.

- To develop an effective interfacial polymerization protocol for preparation of AqpZ/BP1 embedded thin film composite RO membrane.

- To develop a novel biomimetic desalination membrane by covalently crosslink AqpZ to the substrate.

- To investigate the desalination performance of the synthesized biomimetic membranes.

The present thesis comprises of four chapters:

- Chapter 1 presents the motivation, background and scope of this work.

- Chapter 2 discusses the details of the design and fabrication of AQP/peptide complex embedded polyamide RO membrane. Peptide synthesis, preparation of the complex, interfacial polymerization techniques, and characterizations of the biomimetic membrane are presented.

- Chapter 3 introduces another method to embed AQPs into the membrane via click chemistry. Functionalization of the peptide and the polymer, membrane casting techniques, click chemistry reaction and characterizations of the membrane are reported.

- Chapter 4 summarizes results and key conclusions of this thesis. Future prospects based on the outcome of this work are proposed. Further studies to improve the project are also recommended.

Chapter 2 Biomimetic desalination membranes via interfacial polymerization

2.1 Introduction

As introduced in Chapter 1, Tao et al.[43] developed a universal method to improve the stability of membrane proteins using short amphiphilic β-strand peptides. In their experimental part, four membrane proteins that have similar secondary structure with AQPs were tested and all exhibited excellent stability with β-strand peptides. Therefore, in this work, for desalination purpose, the β-strand peptide BP-1 was chosen as the stabilizing agent for AQPs. For AQPs, we used one particular AQPs named AquaporinZ (AqpZ) as the functional water channel protein, because AqpZ can be produced from *E. coli* with relatively high yield[35, 62], and is more stable under different reducing conditions and at temperatures of 4°C[35]. To incorporate the stabilized AqpZ into the membrane system, an efficient embedding technique was required to load AqpZ while minimize defect formation during fabrication and testing.

In this work, interfacial polymerization technique was applied to load AqpZ and form a dense barrier layer to maintain high salt rejection. As discussed in Chapter 1, interfacial polymerization is a type of step-growth polymerization in which polymerization occurs at the interface between an aqueous solution and an organic solution [63]. As the two phases are not miscible, the reaction only occurs at the interface of the two phases. Meanwhile, the acyl chloride monomer in organic phase has very high react activity with amine monomer in aqueous phase, leading to the formation of a dense thin polyamide layer in a very short reaction time.

Due to the highly crosslinked polyamide with small free volume (approximately 0.3–0.5 nm[64]), resulting in high salt rejection of the membrane. Moreover, due to the hydrophilic nature of polyamide and relatively thin barrier layer (several hundred nanometers thick[65]), high water permeability is able to be obtained. In previous research, Zhao et al.[54] encapsulated AqpZ proteoliposomes into the polyamide barrier layer by interfacial polymerization method. The AqpZ molecules was active after incorporating into the aqueous phase of interfacial polymerization reaction, supported by the evidence of water permeability enhancement of the resulting biomimetic membrane. This indicated that the interfacial polymerization is mild enough for AqpZ. In addition, the dense layer protects AqpZ molecules from falling off the membrane and further enhances the mechanical stability of the biomimetic membrane.

In this chapter, we aim to fabricate a robust biomimetic RO membrane by encapsulating AqpZ/BP-1 complex into interfacial polymerization on a porous polysulfone substrate (Figure 2.1). We started with assessing the stability and conformation of AqpZ/BP-1 complex by circular dichroism (CD) and transmission electron microscopy (TEM). AqpZ/BP-1 complex was then introduced in the aqueous phase in the interfacial polymerization reaction. Two conventional reagents, *m*-phenylenediamine and trimesoyl chloride, were used for the reaction. To confirm the function of AqpZ in the casted membrane, an inactive AqpZ variant (i.e., a mutant with low water permeability) is used as a negative control. Desalination performances of the two membranes were compared, along with other controls. Moreover, different amount of the complex were added into the membrane to study the effect on membrane performance. This new strategy allow me to fabricate a novel mechanical robust biomimetic desalination membrane that exhibits excellent water permeability, salt rejection and high tolerance for high

testing pressure. Moreover, it is scalable in practice, which makes it a potential candidate for industrial development.

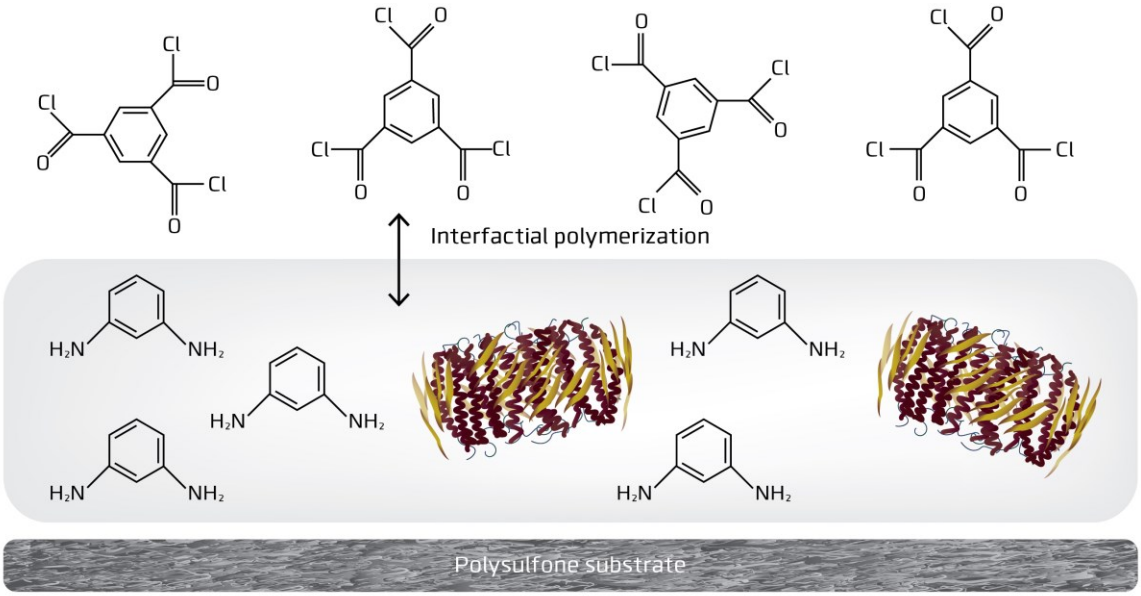

Figure 2.1 Scheme of the synthesis of an AqpZ/BP-1 complex incorporated biomimetic membrane (top layer: trimesoyl chloride in organic phase; second layer: *m*-phenylenediamine and AqpZ/BP-1 complexes in aqueous phase; and the interfacial polymerization reaction occurs at interface of aqueous and organic phases on top of polysulfone substrate.)

2.2 Experimental methods

2.2.1 Materials

- Materials for peptide synthesis and AqpZ expression and purification

Rink amide AM resin with 0.52mmol/g substitution, N-Fmoc-L-aspartic acid beta-tert-butyl ester (Fmoc-Asp(OtBu)-OH), N-Fmoc-O-t-butyl-L-serine (Fmoc-Ser(tBu)-OH), N-Fmoc-L-leucine (Fmoc-Leu-OH), (2-6-chloro-1H-benzotriazole-1-yl) -1,1,3,3-

tetramethylaminium hexafluorophosphate (HCTU) with purity over 98% were purchased from AAPPTec. Amino acids (S)-N-Fmoc-octylglycine with the purity of 98% was purchased from ACROS Organics. N, N-diisopropylethylamine (DIEA) with purity of 99.5%, trifluoroacetic acid (TFA) with purity of 99%, triisopropylsilane (TIS) with putity of 98% and piperidine with purity of 99.5% were purchased from Sigma-Aldrich. Anhydrous solvents, 99.8% dimethylformamide (DMF), 99.8% methanol, and 99.0% ether were ordered from Sigma-Aldrich as well.

Both activeAqpZ and inactiveAqpZ were expressed and applied in this work. The inactiveAqpZ refers to the mutant with low water permeability and it is regarded as the negative control to the activeAqpZ. AqpZ was expressed from *E.coli* and purified by using Ni-NTA affinity chromatography. All the expression and purification of AqpZ was performed according to the previously reported protocol[35] with minor modifications by the Bio-team colleagues.

- Chemicals for membrane synthesis and characterization

Reagents for interfacial polymerization: *m*-phenylenediamine (MPD) with 99% purity, trimesoyl chloride (TMC) with 98% purity, triethylamine (TEA) with 99% purity, and salt: sodium chloride (NaCl), monosodium phosphate (NaH_2PO_4) with purity over 98% were purchased from Sigma-Alderich. Hexane with purity of 98.5% was purchased from Fisher Scientific. The supporting membrane UE50 was ordered from sterlitech.

For structure characterization of the protein/peptide complex, 1.8 nm and 5 nm Ni-NTA-nanogold, and 1.4 nm Mono-Sulfo-NHS-nanogold were bought from Nanoprobes for labeling protein and peptide respectively.

2.2.2 Peptide synthesis

The peptides were synthesized via Fmoc stractegy [66, 67] using Rink Amide AM resin following by the sequence as acetyl-(octyl)Gly-Ser-Leu-Ser-Leu-Asp-(octyl)Gly-Asp-NH_2. Manually, the steps are as follows (Figure 2.2):

(1) Swell. Swell the resin with DMF and shake for 1 hour.

(2) Deprotection. Mix resin and 20% piperidine in DMF solution and shake for 10 mins. Filter out the solution and repeat again.

(3) Wash. Wash the resin with the sequence of 4 times DMF, 4 times methanol and 4 times DCM.

(4) Coupling. Prepare coupling solution of HCTU (4 eq.), DIEA (8 eq.) and amino acid (4 eq.) in DMF. Mix the solution with resin, and shake for 2 hours. For the next amino acid coupling, repeat from step (3).

(5) Acetylation. After finishing all the amino acid coupling and last wash and swell, mix resin with acetic anhydride (10%) and DIEA (2-5%) in DMF. Shake for 15 minutes and wash with DMF 3 times.

(5) Cleavage. Prepare cleavage cocktail with 95% TFA, 2.5% TIS and 2.5% DI water. Mix with resin and shake for 3 hours. Filter the resin out and collect the solution. Participate peptide in ether.

The peptide was then purified by reverse-phase HPLC (CH_3CN-H_2O, 0.1% TFA) and dried by freeze dryer. Similarly, for large amount of BP-1 synthesis, peptide synthesizer (Infinity 2400 and Focus XC from Aapptec) was used to synthesize BP-1. The molecular weight of BP-1 was

confirmed by Electrospray ionisation mass spectrometry (ESI-MS) (Agilent 1946 LC/MS).

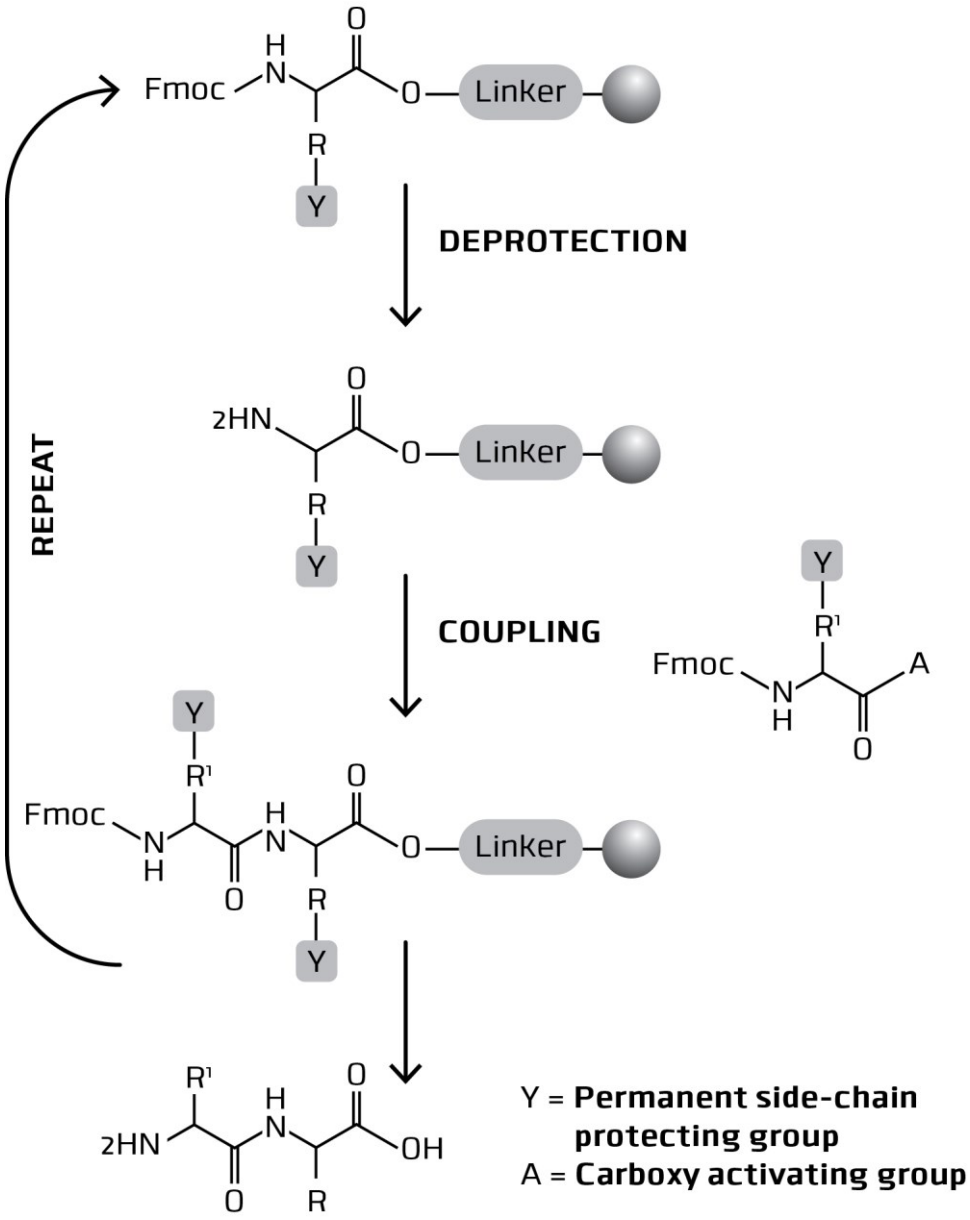

Figure 2.2 Flow chart of the solid phase peptide synthesis.

2.2.3 Protein wrapping and AqpZ/BP-1 complex formation

After expressed and purified from *E. coli*, AqpZ was stabilized by *n*-Dodecyl-β-D-

maltopyranoside (DDM) in buffer solution. The protein concentration was detected by Direct Detect infrared spectrometer (EMD Millipore). In the protein wrapping procedure, BP-1 was first mixed with the purified AqpZ at a 50:1 molar ratio. It is expected that BP1 will replace DDM and cover around the hydrophobic surface of AqpZ. DDM was subsequently removed by dialysis against detergent-free buffer (10 mM NaH_2PO_4, pH 7.4) using a 10 kDa cut-off membrane. Dialysis was performed at 4 °C for 1–2 days. The process of BP-1 stabilizing AqpZ, and replacing the detergent molecules is shown in Figure 2.3. The resulting AqpZ/BP-1 complex structure was studied by CD and TEM.

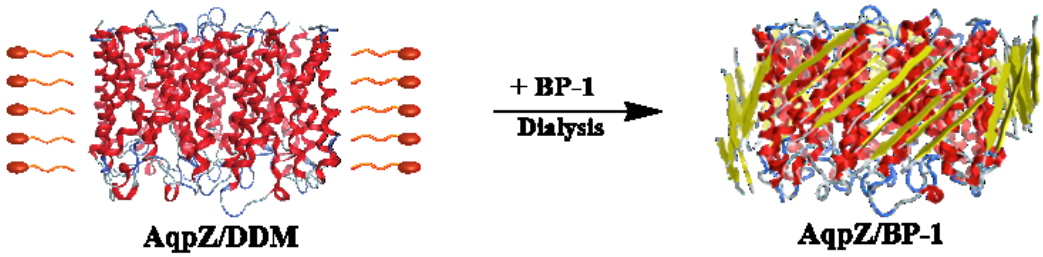

Figure 2.3 Schematic representation of the process of BP-1 replacing DDM to wrap around AqpZ, forming tight β-barrel structure.

2.2.4 Interfacial polymerization

In order to form a dense salt rejection polyamide layer, MPD and TMC were used as monomers for interfacial polymerization[68]. AqpZ/BP-1 complex was added to create preferential water paths in the polyamide barrier layer (Figure 2.1). The general procedure was (Figure 2.4): The polysulfone substrate was first soaked in a 2 wt% MPD aqueous solution with 2 wt% TEA, and 4mg/ml AqpZ/BP-1. The excess aqueous solution was removed by compressed nitrogen gas. 0.1 wt% TMC hexane solution was then gently poured on to the substrate surface

to react with the residue MPD for 30s. After pouring out extra organic phase solution from membrane surface, the membrane was kept in 60ºC oven for 10mins as post-treatment. Two different sets of membranes were prepared according to Table 2.1 and Table 2.2.

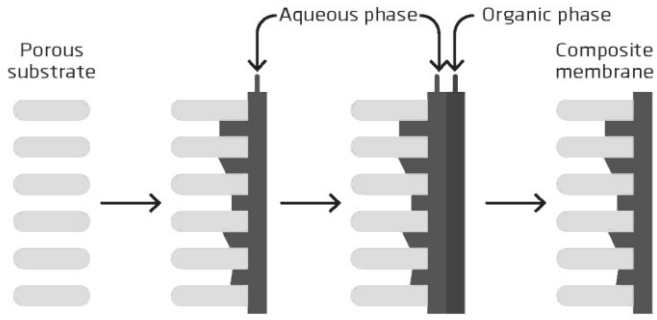

Figure 2.4 Typical procedures for interfacial polymerization to fabricate polyamide barrier layer on top of a porous substrate.

Table 2.1 Interfacial polymerization conditions for fabricating M_0, M_{BP1}, $M_{inactive}$, and M_{active}.

Sample ID	Sample	Aqueous phase		Oil phase
		Chemicals	AqpZ complex amount per 30 ml reaction	
M_0	Conventional TFC membrane	2 wt% MPD, 2 wt% TEA	N/A	0.1 wt% TMC
M_{BP1}	BP-1-TFC membrane	2 wt% MPD, 2 wt% TEA	0.115 mg BP-1 (38.3 ul 3 mg/mL BP-1 solution, same amount of BP-1 as in the following membranes)	0.1 wt% TMC
$M_{inactive}$	inactiveAqpZ/BP-1-TFC membrane	2 wt% MPD, 2 wt% TEA	0.1 mg inactiveAqpZ/BP-1 (25 ul 4 mg/mL inactiveAqpZ/BP-1 solution)	0.1 wt% TMC
M_{active}	activeAqpZ/BP-1-TFC membrane	2 wt% MPD, 2 wt% TEA	0.1 mg activeAqpZ/BP-1 (25 ul 4 mg/mL activeAqpZ/BP-1 solution)	0.1 wt% TMC

Table 2.2 Interfacial polymerization conditions for fabricating a series of membranes with adding different amount of AqpZ/BP-1 complex in aqueous phases.

Sample ID	Sample	Aqueous phase		Oil phase
		Chemicals	AqpZ complex amount per 30ml reaction	
M_0	Conventional TFC membrane	2 wt% MPD, 2 wt% TEA	N/A	0.1 wt% TMC
M_1	0.025 mg activeAqpZ/BP-1-TFC membrane	2 wt% MPD, 2 wt% TEA	0.025 mg activeAqpZ/BP-1	0.1 wt% TMC
M_2	0.05 mg activeAqpZ/BP-1-TFC membrane	2 wt% MPD, 2 wt% TEA	0.05 mg activeAqpZ/BP-1	0.1 wt% TMC
M_3	0.075 mg activeAqpZ/BP-1-TFC membrane	2 wt% MPD, 2 wt% TEA	0.075 mg activeAqpZ/BP-1	0.1 wt% TMC
M_4	0.1 mg activeAqpZ/BP-1-TFC membrane	2 wt% MPD, 2 wt% TEA	0.1 mg activeAqpZ/BP-1	0.1 wt% TMC
M_5	0.3 mg activeAqpZ/BP-1-TFC membrane	2 wt% MPD, 2 wt% TEA	0.3 mg activeAqpZ/BP-1	0.1 wt% TMC

2.2.5 Characterizations

- **Characterizations of AqpZ/BP-1 complex**

Jasco J-810 CD Spectropolarimeter (Jasco, Japan) was utilized to investigate the secondary structures of BP-1, AqpZ and AqpZ/BP-1 complex. Samples were all prepared in 10 mM NaH_2PO_4 buffer with pH 7.4. The CD experiments were performed under scanning wavelength from 190 nm to 260 nm with1.0 nm step, 1.0nm bandwidth and a 3s collection time per step at 25ºC in a 0.1 cm pathlength quartz cell. The structure of AqpZ/BP-1 complex was also studied

by using JEM-2200FS transmission electron microscope. As shown in Table 2.3, different part of the complex was labeled by gold nanoparticles to get a better contrast under TEM observation. TEM samples of the above were diluted to around 0.05 mg/ml and dropped onto freshly glow discharged carbon-coated copper grids for 30s. The excess liquid was then blocked from the grid. High-angle annular dark-field mode was used for observation.

Table 2.3 The preparation of nanogold labeled AqpZ/BP-1 TEM samples

Sample ID	Nanogold AqpZ complex labeling	
	AqpZ	BP-1
S1	AqpZ was labeled by 1.8 nm gold nanoparticles	Not labeled
S2	Not labeled	BP-1 labeled with 1.4 nm gold nanoparticles
S3	BP-1 was labeled with 1.4 nm gold nanoparticles	AqpZ was labeled by 5 nm gold nanoparticles.

- **Characterization of membrane surfaces**

Zeiss Sigma Field Emission Electron Microscope (Zeiss, Germany) was used to observe the morphology of membranes. To prepare the SEM sample, the membrane was dried under vacuum overnight under 25ºC and coated with a ~5 nm thick gold to minimize the charging effect. Observation was performed under 5 kV and in-lens state.

2.2.6 RO membrane performance test

Desalination properties of the resulting biomimetic membranes were characterized in a standard crossflow reverse osmosis setup (customized by Sterlitech). Firstly, the testing membrane was placed into the testing cell with 42 cm^2 active surface area (CF42 membrane cell, Sterlitech). The feed solution (1 g/L NaCl at 25ºC) was pumped at a constant cross flow 0.8

gallon per minute (GPM). Membranes were compacted for 1 h at 200PSI before water flux and rejection measurements. The water flux (J_w) was calculated from collected permeate volume at a unit time on a unit membrane area ($(\frac{\text{Liter}}{m^2 \times hour})$, LMH).The salt rejection (R) was obtained from the conductivity differences between the feed solution and the permeate solution by using a conductivity meter (inlab 741, mettle toledo), ($R = 1 - C_p/C_f$). According to the following equations, the water permeability coefficient (A) and salt permeability coefficient (B) can be calculated. [69]

$$A = \frac{Jw}{\Delta P - \Delta \pi} \quad \text{B} = J_W \times (\frac{1}{R} - 1)$$

2.3 Results and discussion

2.3.1 Structure and stability study of BP-1 and AqpZ/BP-1 complex

After BP-1 was synthesized and purified, BP-1 was verified by ESI-MS. Two main peaks, m/z 1043.89 (1043.29 calcd for [BP-1+H^+]) and m/z 1065.87 (1065.27calcd for [BP-1+Na^+]) were observed from the spectrum, which confirmed the correct identity of BP-1. From the circular dichroism spectroscopic analysis of BP-1 in aqueous phase (Figure 2.5), the signal at 219 nm indicated the formation of β-sheet secondary structure. Compared to a typical β-sheet signal at 218nm, a slightly redshift was observed from this result. The redshift may result from a conformational distortion due to the N-methylated group in the middle of peptide backbone [70] [71].

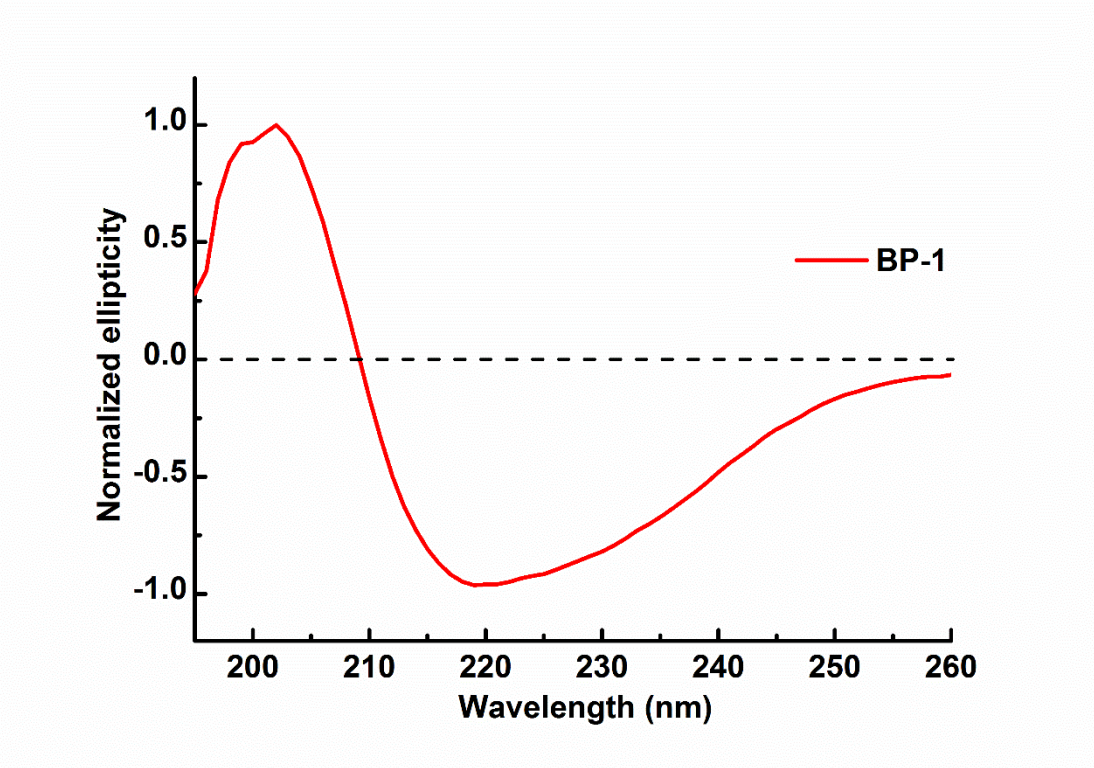

Figure 2.5 CD spectrum of BP-1 in aqueous solution.

After dialysis procedure to remove DDM, the stability of AqpZ/ BP-1 complex was studied by CD. Control sample without any BP-1 experienced same dialysis procedure to get rid of DDM. As shown in Figure 2.6 red line, AqpZ/BP-1 complex sample maintained alpha-helix structure of AqpZ with characteristic alpha-helix ellipticity signals at 193 nm, 208 nm and 220 nm[72]. However, the control sample of AqpZ/DDM-free (black line in Figure 2.6) was not able to maintain a predominant alpha-helix structure after same dialysis procedure, which reveals that without the protection from BP-1 the AqpZ secondary structure was partly destroyed. Therefore, compared with more loosely bound and less ordered detergent molecules, BP-1 appeared to be a better stabilizing agent. We expected that it might result from the tight binding between BP-1 and AqpZ by hydrophobic force and BP-1 self assembled around AqpZ to form

β-sheet structure by intermolecular hydrogen-bonding between the BP-1 molecules.

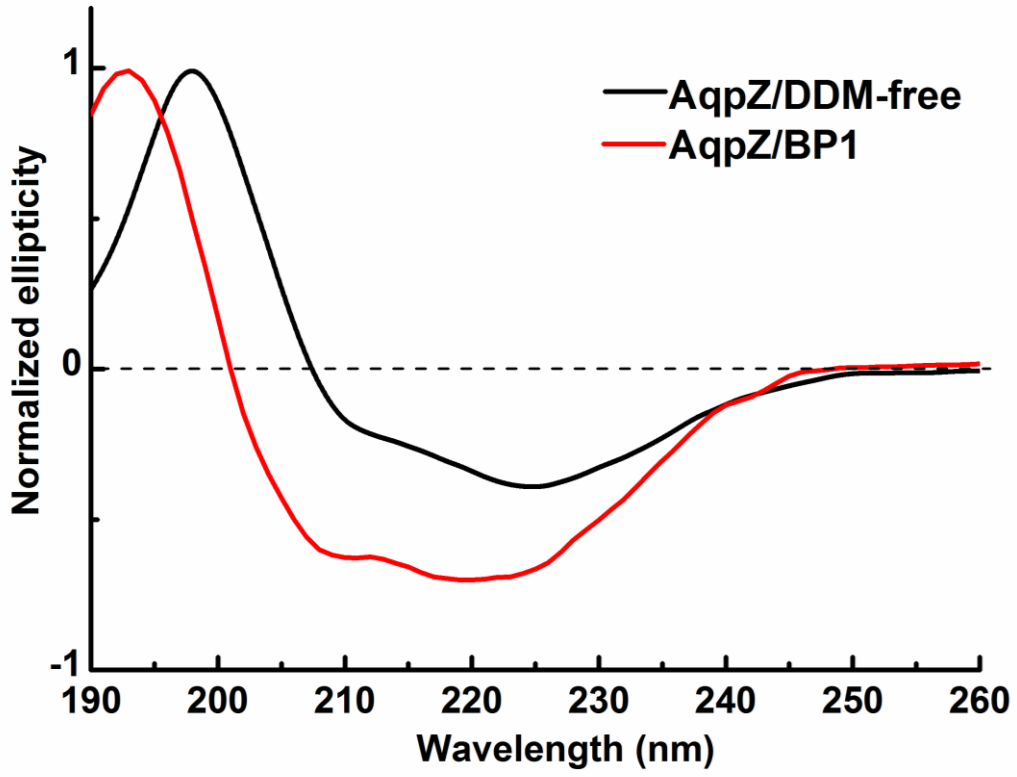

Figure 2.6 CD spectra of AqpZ/DDM-free (black line), and AqpZ/BP-1 (red line) after dialysis.

AqpZ/BP-1 complex structure was studied by TEM as well. For better contrast, different part of the complex was labeled by different size of gold nanoparticles. Firstly, AqpZ/BP-1 complex was labeled with 1.8 nm gold nanoparticles functionalized with NTA. NTA allows the gold nanoparticle to specifically bind to AqpZ. TEM image of the AuNP-AqpZ/BP1 sample reveals that the protein-peptide complex is well dispersed in aqueous phase that no aggregation was observed (Figure 2.7a). This confirms BP1 is able to stabilize AqpZ in detergent-free

aqueous buffer. Subsequently, BP-1 labeled with 1.4 nm gold nanoparticles was used to form AqpZ/AuNP-BP1 complex. TEM image of this sample shows that there are around 18-60 copies of BP-1 in a AqpZ/BP1 complex (Figure 2.7b). Secondary structure of the BP1 is not distinguishable by this method. In Figure 2.7c, BP-1 and AqpZ were each labeled with different size of gold nanoparticles. AqpZ was labeled by 5 nm gold nanoparticles and BP-1 was labeled by 1.4 nm gold nanoparticles. In this case, clusters of 5 nm AuNP with multiple 1.4 nm AuNP were observed, confirming the assembly of AqpZ and BP1 peptides. Similar to previous observation, no aggregation of 5 nm AuNP was found and accordingly BP1 prevents AqpZ from aggregating. Overall the TEM study confirms that BP-1 was able to assemble around AqpZ and stabilize it.

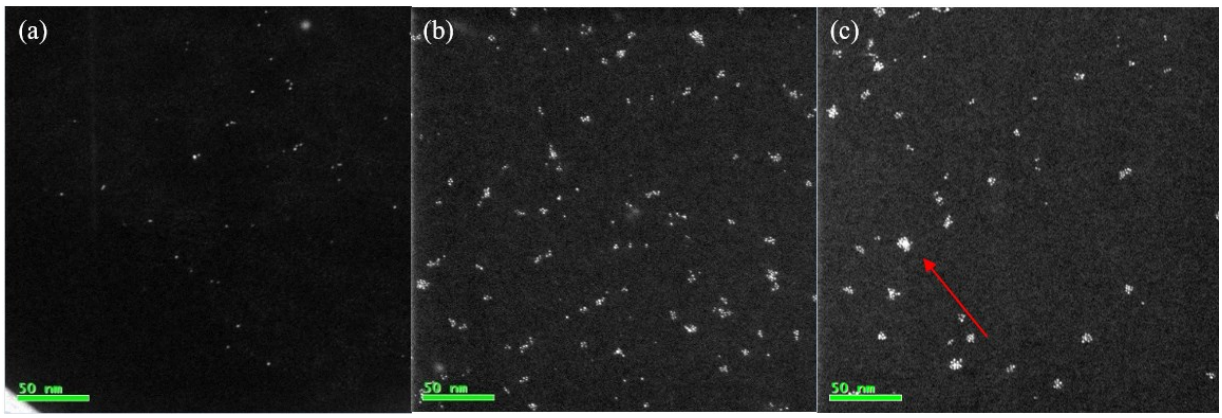

Figure 2.7 TEM images of AqpZ/BP-1 complex for structure study. (a) AqpZ/BP-1 complex of AqpZ was labeled by 1.8 nm gold nanoparticles; (b) AqpZ/BP-1 complex of BP-1 labeled by 1.4 nm gold nanoparticles; (c) AqpZ/BP-1 complex of AqpZ labeled by 5 nm gold nanoparticles and BP-1 by 1.4 nm gold nanoparticles. The red arrow is pointed at one single AqpZ/BP-1 complex. (The TEM images were obtained by Julie Qian)

For long term stability study, a AqpZ/BP-1 sample was store at 4 ºC for 4 weeks and its secondary structure of monitored by CD weekly. As shown in Figure 2.8, the complex

maintained its secondary structure over the observation period. The sample remained well dispersed and no aggregation was observed after centrifugation (4000 rpm for 10 min).

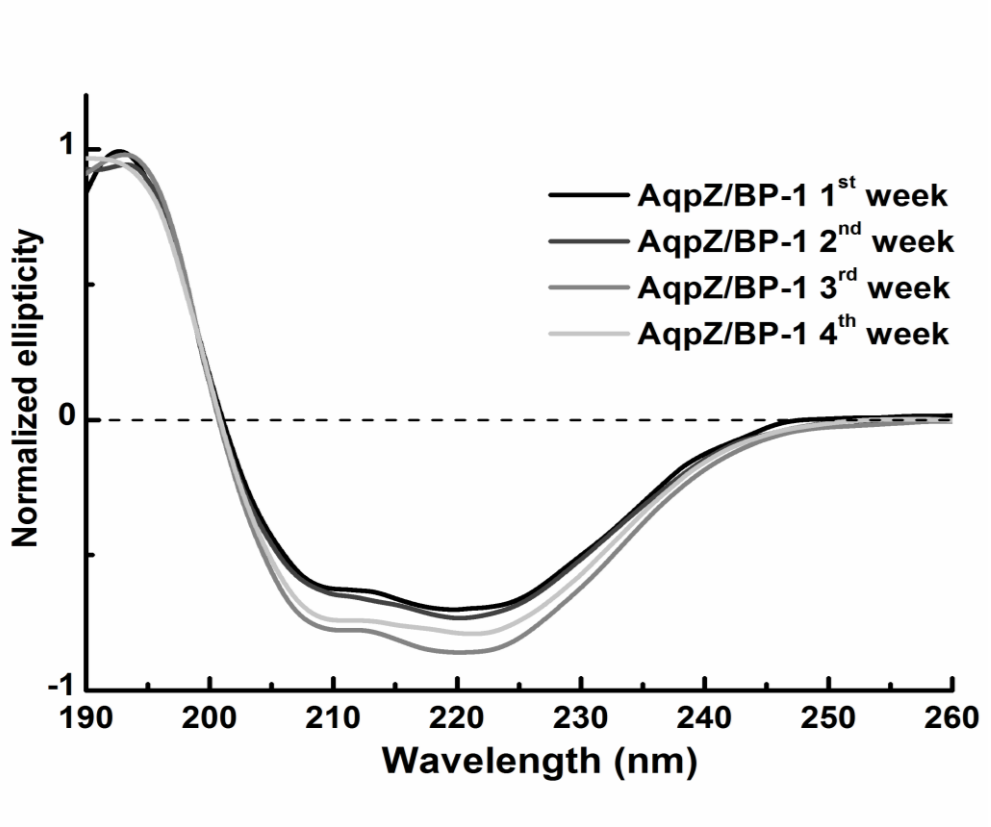

Figure 2.8 CD spectra of AqpZ/BP-1 complex over a four-week period.

2.3.2 Surface morphology study of TFC membranes

In order to demonstrate that AqpZ has the ability to increase water permeability while maintaining the salt rejection, a set of membranes were prepared using different reaction conditions as summarized in Table 2.1. By comparing the surface morphology and desalination performances of the membranes, the function of AqpZ/BP-1 complex in membrane system is testified.

Figure 2.9 presents the SEM micrographs of support substrate UE50, M_0 (conventional TFC membrane without AqpZ and BP-1), M_{BP-1} (TFC membrane with BP-1), $M_{inactive}$ (TFC membrane with inactiveAqpZ/BP-1 complex), and M_{active} (TFC membrane with activeAqpZ/BP-1 complex). The UE50 (Figure 2.9a) had a relatively smooth surface compared with membranes after interfacial polymerization. All other 4 types of membranes had rougher surface due to the presence of unique ridge-and–valley structures that were characteristic for polyamide based RO membranes[73]. However, M_0 membrane (Figure 2.9b and c) exhibited many tightly packed, small nodular structures and less surface roughness and "leaf" like structure, compared to other TFC membranes (Figure 2.9d, e, f, g, h and i). M_{BP-1}, $M_{inactive}$ and M_{active} had similar surface morphologic structure and surface roughness.

The only difference between M_0 and other TFC membranes is the presence of BP-1 in aqueous phase of interfacial polymerization. According to pervious research, interfacial polymerization occurs mostly in the organic phase as the relatively low solubility of TMC in aqueous phase [74, 75]. Due to the amphiphilic inherent property of BP-1, it builds a better connection between the relatively hydrophobic polysulfone substrate and MPD, which indicates that BP-1 improves the absorption of MPD on the support. Therefore, during the interfacial reaction, more MPD would be able to react with TMC in organic phase [76, 77]. Meanwhile, amphiphilic agent could facilitate the mass transfer of diamine molecules to the organic phase[68], which means that BP-1 has the capability to help MPD penetrate more rapidly and deeply into TMC layer. Therefore, the presence of BP-1 enlarges the polymerization area and increases the surface roughness of the resulting TFC membrane[78]. The surface morphology images of the M_{active} and $M_{inactive}$ suggests that the presence of protein-BP-1 complex has similar

effects to BP-1. However, the presence of the complex cannot be directly observed from SEM as the size of the complex was too small.

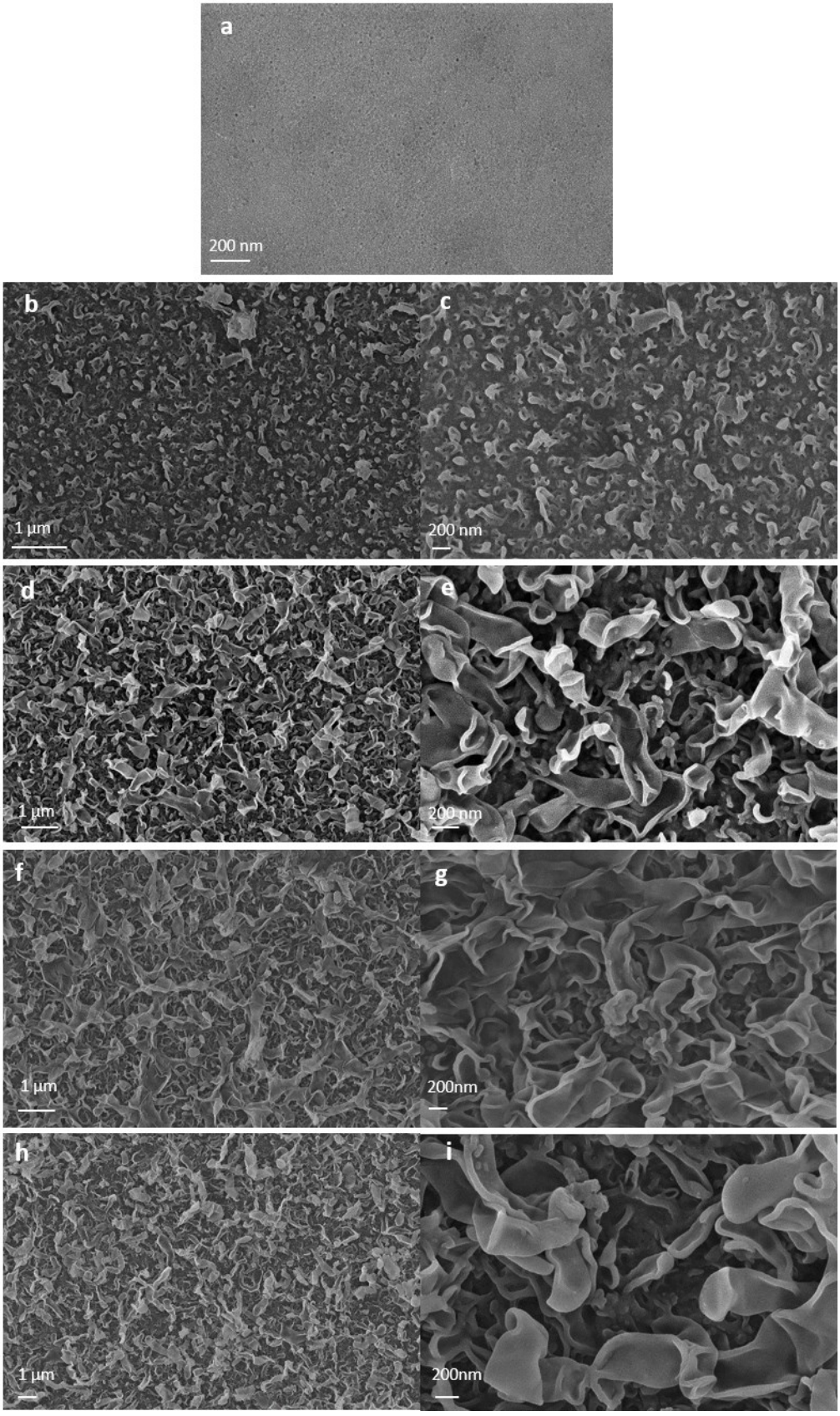
a
200 nm
b
1 µm
c
200 nm
d
1 µm
e
200 nm
f
1 µm
g
200nm
h
1 µm
i
200nm

Figure 2.9 SEM images of (a) UE50 substrate for interfacial reaction; (b, c) top view of M_0 (TFC membrane without AqpZ and BP-1); (e, f) top view of M_{BP-1}, (TFC membrane withBP-1); (d) top view of $M_{inactive}$, (TFC membrane with inactiveAqpZ/BP-1 complex) and (g, h) top view of M_{BP-1}, (TFC membrane with activeAqpZ/BP-1 complex)

2.3.3 Effect of AqpZ/BP-1 complex on membrane performances

The water performance of membranes was evaluated in a cross-flow machine using NaCl (1 g/L) as the feed solution and 200 PSI as the testing pressure. The water flux and salt rejection of M_0, M_{BP-1}, $M_{inactive}$ and M_{active} are summarized in Figure 2.10. The water permeability coefficient (A) was calculated and listed in Table 2.4. Compare M_0 and M_{BP-1}, the water flux increased and salt rejection slightly decreased after adding BP-1 into aqueous phase of interfacial polymerization reaction. As discussed above, the presence of BP-1 in aqueous phase resulted in more rapid and deep mass transfer of MPD into TMC layer, leading to the formation of a thin barrier layer with large membrane area. On the other hand, BP-1, as an amphiphilic agent, decreased the surface tension between two phases, resulting in more TMC hydrolyzed in the organic phase. The hydrolysis of TMC inhibited the crosslinking reaction between the two monomers. Therefore, taking both effects into consideration, adding BP-1 led to the production of a thin but less crosslinked membrane [68] with larger surface area. Less crosslinked barrier layer resulted in higher water flux and slightly decreased salt rejection. Meanwhile, larger surface area provided more interaction area for water molecules to diffuse through the barrier membrane, which also contributed to the increase of water flux. Therefore, adding BP-1 could lead to increase in water flux and slight decrease in salt rejection.

$M_{inactive}$ had comparable water permeability to M_{BP-1}, whereas M_{active} had much higher

water permeability. According to Table 2.4, M_{active} was 28% more permeable compared to $M_{inactive}$ and 84% more compared to M_0. Both $M_{inactive}$ and M_{active} were able to maintain a high salt rejection under 200 PSI. It indicates that no defects were formed during the process of introducing AqpZ/BP-1 complex into the interfacial polymerization. Accordingly, the increase in water flux in M_{active} can only be attributed to the presence of activeAqpZ/BP-1 complex in the membrane. This suggests that the activeAqpZ/BP-1 complex was stable and functional in the barrier layer, and that BP-1 is an effective stabilizing agent for AqpZ. The membrane was able to maintain its performance over time, which reveals that the complex was well protected by polyamide layer from peeled off the membrane surface. Meanwhile, the whole biomimetic membrane was able to withstand high RO testing pressure, indicating the mechanically robustness of the membrane. This study clearly demonstrates the potential of preparing high performance biomimetic membranes using AqpZ/BP-1 complex in an interfacial polymerization system.

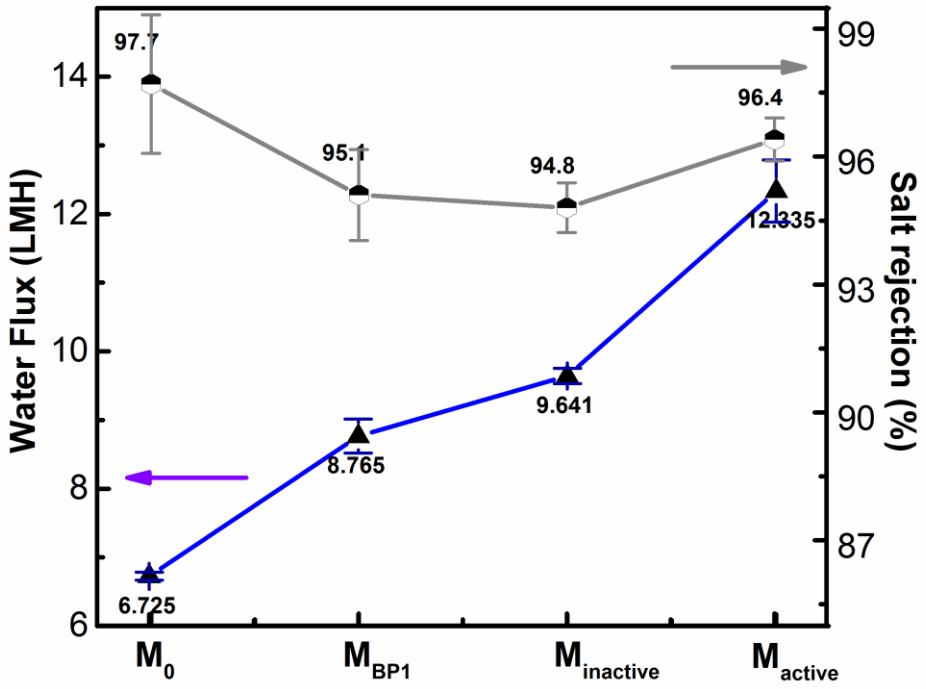

Figure 2.10 Water flux (blue line) and NaCl rejection (grey line) of M_0, M_{BP-1}, $M_{inactive}$ and M_{active} at an applied pressure of 200PSI. The feed solution contained 1g/L NaCl.

Table 2.4 The Water permeability coefficient (A) of TFC membranes

	M0	MBP1	Minactive	Mactive
Water permeability coefficient A (LMH/Bar)	0.488	0.636	0.699	0.895

2.3.4 Effect of adding amount of AqpZ complex on membrane performances

The effect of AqpZ/BP-1 complex adding amount on membrane performance was also investigated in this chapter. As shown in Table 2.2, different amount of AqpZ/BP-1 complex

was added into aqueous phase during interfacial polymerization, resulting in different amount of complex incorporated in membrane system.

As shown in Figure 2.11, the water flux enhanced linearly with increasing adding amount of AqpZ/BP-1 complex (black line) or BP-1 (red line) in the aqueous phase. It is noticed that when same molar amount was added into the reaction, membrane with AqpZ/BP-1 complex always provides a better water permeability (in Figure 2.11, the slope of black line is larger than the slope of red line) than membrane with BP-1 only. This suggests that AqpZ acts as a highly permeable water channel in the polyamide layer. However, the linear relation between adding amount of AqpZ/BP-1 complex and water flux was only valid under low adding amount (below 0.1 mg). When adding 0.3 mg of AqpZ/BP-1 complex into the reaction, the experimental value of water permeability was 15.27±1.31 LMH, which was much lower than the extrapolated value of 22.19 LMH. A reasonable explanation is: during the interfacial polymerization process, AqpZ/BP-1 complex and MPD were only interacted with polysulfone substrate by Van der Waal's force[79], and extra aqueous solution with monomers were poured out. That suggests that in a certain membrane surface area, the substrate only allows to absorb certain amount of AqpZ/BP-1 complex. In this case, with increasing amount of the complex in aqueous phase, the absorption on the surface reached its maximum value. Consequently, the AqpZ complex in resulting polyamide barrier layer reached its maximum value. Therefore, the increasing amount of the complex in aqueous phase was no longer able to enhance the water permeability.

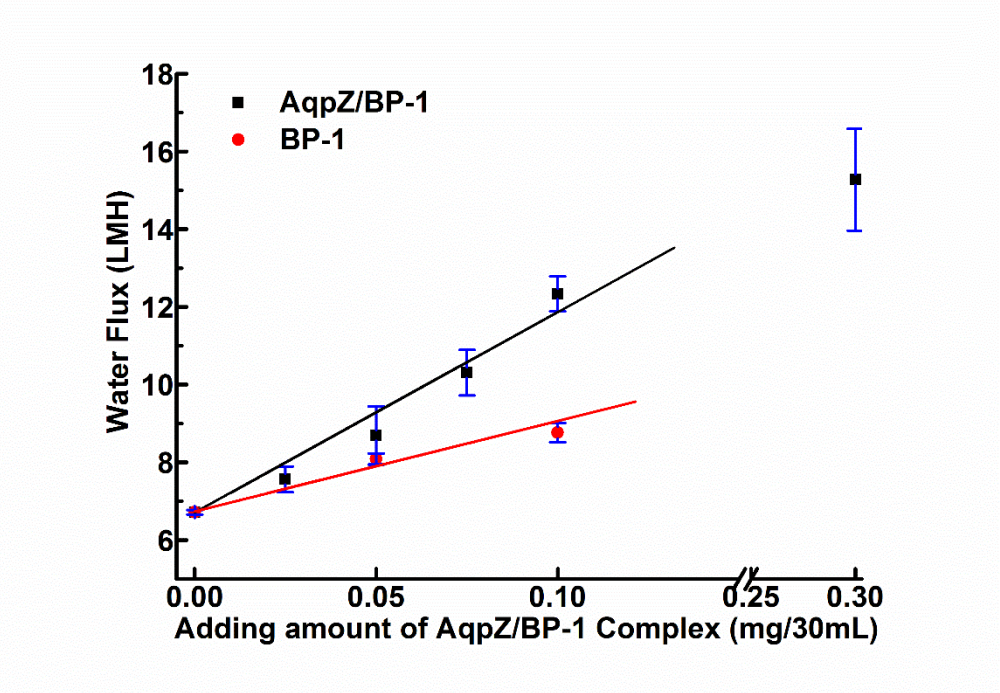

Figure 2.11 Effect of mass amount of AqpZ/BP-1 (black line) and BP-1 (red line) on membrane water permeability performance. (Note that there is a break in x-axis)

2.4 Conclusion

In this chapter, a novel technique using amphiphilic peptide to stabilize AqpZ was applied into biomimetic membrane fabrication. The AqpZ/peptide complex was well stabilized in aqueous solution and was able to be successfully incorporated into the barrier layer of membrane by interfacial polymerization reaction. The resulting membrane exhibited good mechanical stability that can withstand 200 PSI pressure under RO conditions. The water permeability was highly increased without sacrificing the salt rejection, which also indicates that the complex has the ability to stabilize AqpZ and maintain its function within the membrane. This membrane design also shows great potential for industrial scale production as it is easy to scale up to

produce large defect-free membrane in a continuous casting. The results reported here are very promising, however, more studies are required to further enhance the incorporation efficiency of AqpZ/BP-1 complex in the membrane.

Chapter 3 Biomimetic membrane via click chemistry

3.1 Introduction

After demonstrated that the amphiphilic peptide was an effective tool to stabilize AqpZ, we came up with a new idea of using functional peptide to control the loading of the protein on the membrane support. A successful ligation between functional protein/peptide complex and the porous substrate should meet the following requirements: high selectivity, inert to other functional groups, compatibility with aqueous solution, and high yield. Click chemistry, regarded as a 'set of powerful, highly reliable, and selective reactions for the rapid synthesis of useful new compounds and combinatorial libraries'[80], is one potential method for the ligation of polymer and protein in the biomimetic membrane design.

Click chemistry represents a range of reactions with different reaction mechanisms but common reaction trajectories, such as the copper-catalyzed 1,3 dipolar cycloaddition[80, 81], Diels-Alder reaction[82], Thiol-ene reaction[83] and so on. The most widely used method among click chemistry is copper-catalyzed azide–alkyne cycloaddition (CuAAC)[84]. Figure 3.1 shows the typical CuAAC reaction occurred between alkynyl and azide reagents. It has several advantages for application in a biological system: the alkynyl and azide group are inert to other functional groups in living systems, the click reaction is generally compatible with aqueous media near physiological pH and at room temperature to prevent destruction of biological molecules[61], and high yield even when the concentrations of manipulated biomolecules are low[85]. Although the catalyst copper might be a concern in a biological system, optimized CuAAC reaction has been developed and applied to bioconjugation. For

example, Nolte *et al*.[86] successfully built up a biohybrid amphiphilic system by using CuAAC method to click the terminal azide functionalized polystyrene with an alkynyl functionalized transport protein bovine serum albumin (BSA). Given the advantages and feasibility of CuAAC reaction, it was chosen as the chemistry for crosslinking the protein/peptide complex and the polymer substrate. For this purpose, we prepared alkynyl functionalized BP-1 and azide-functionalized polysulfone substrate.

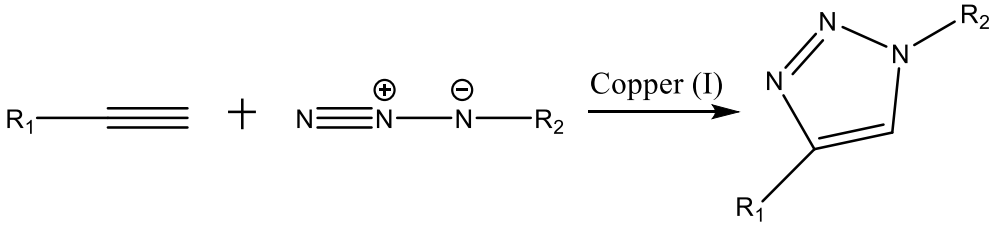

Figure 3.1 The framework of CuAAC

In this chapter, a novel biomimetic membrane fabrication strategy was presented by using alkynyl functionalized peptide to stabilize and load AqpZ onto azide modified polymer support via biocompatible click chemistry (Figure 3.2). Based on BP-1 structure, the alkynyl functionalized peptide can be easily modified by adding a functional amino acid with alkynyl group into the peptide sequence. As shown in Figure 3.3, a propargylglycine amino acid was incorporated into the BP1 sequence at the ninth position. The modified peptide was synthesized using solid phase peptide synthesis. Because of the inert and bio-orthogonal property of alkynyl group, the propargyl side group does not react with the reagents or inhibit the solid phase synthesis[87]. Polysulfone was chosen as the starting material for the substrate because it is widely available and can be readily modified. It is also highly thermostable and resistant to mechanical, chemical, and bacterial attack. Polysulfone can be functionalized with azide group

on the side chain with two steps. The product was then applied to cast a substrate with appropriate pore size[88] using liquid-induced phase inversion technique. The biomimetic membrane was subsequently prepared by clicking the AqpZ/propargyl functionalized peptide (FBP-1) complex to the porous azide-functionalized polysulfone substrate.

The functionality of the alkynyl group of FBP-1, the stability of AqpZ/FBP-1 complex, the immobilization of AqpZ/FBP-1 complex onto azide-functionalized substrate via click chemistry, and preliminary study on the desalination performance, were investigated in this chapter.

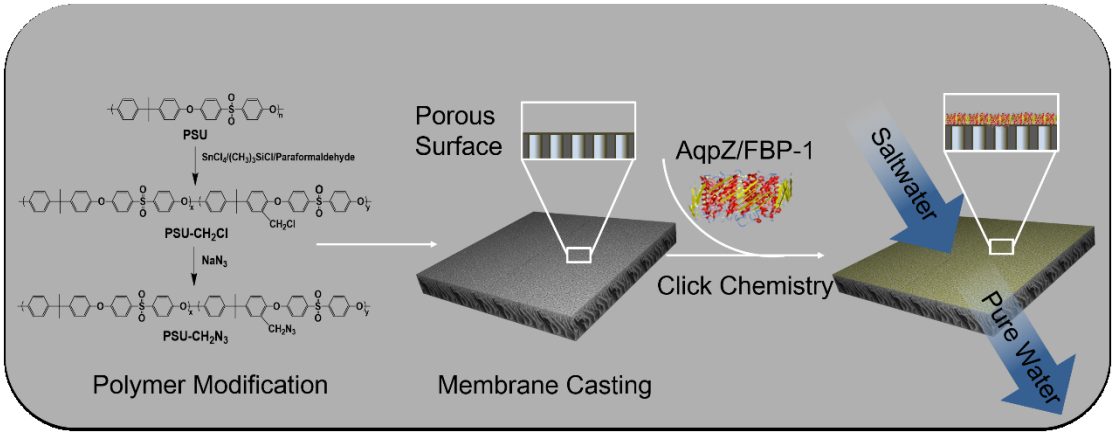

Figure 3.2 Schematic illustration of AqpZ/FBP-1 membrane fabrication

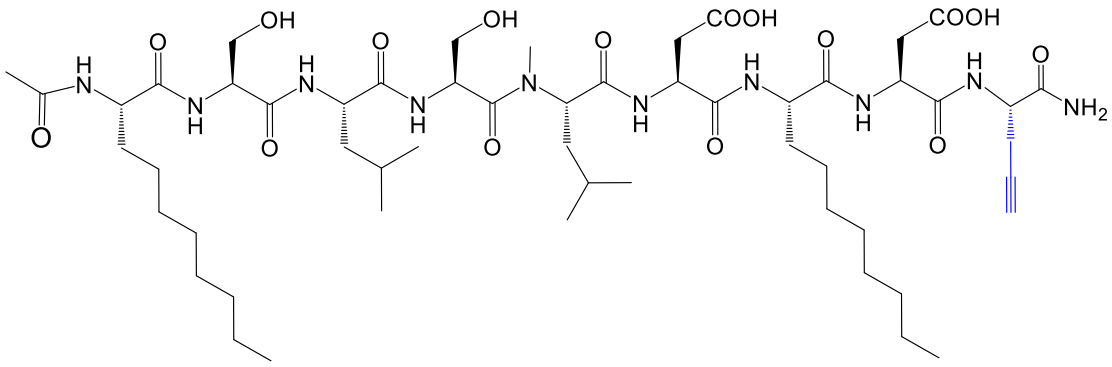

Figure 3.3 The chemical structure of FBP-1. The alkyne functional group is highlighted in blue.)

3.2 Experimental methods

3.2.1 Materials

- Materials for AqpZ, FBP-1 synthesis and characterization

Apart from the chemicals required to synthesis peptide in Chapter 2, amino acid Fmoc-L-2-propargylglycine with purity of 98% was purchased from Sigma-Aldrich. For peptide characterization purpose, red-fluorescent Tetramethylrhodamine 5-Carboxamido-(6-Azidohexanyl) (TAMRA Azide) was purchased from Life technologies.

AqpZ was expressed and purified followed by same protocol mentioned in chapter 2. For characterization and observation, Click-iT® protein reaction buffer kit, and fluorescein (FITC) were purchased from Life Technologies (Thermo Fisher Scientific).

- Materials for polymer modification and membrane casting

Udel P-1700 polysulfone (PSU) with molecular weight of 19800 Da and 1.75 PDI (the polydiversity index, M_w/M_n) was received from Solvay. Paraformaldehyde with purity of 95%, chlorotrimethylsilane with purity of 99%, tin (IV) chloride with purity of 98%, sodium azide with putify of 99% were purchased from Sigma-Aldrich. Solvents such as chloroform, methanol, N-Methyl-2-and pyrrolidone(NMP) with purity higher than 99% were purchased from Fisher Scientific. Pore agent Polyvinylpyrrolidone K 30, with average M_w 40000 was ordered from Sigma-Aldrich.

- Materials for click chemistry

Click chemistry reagents including copper (II) sulfate, N,N,N',N'',N''-

Pentamethyldiethylenetriamine (PMDETA), and sodium ascorbate with purity of 99% were purchased from Sigma-Aldrich.

3.2.2 FBP-1 synthesis and protein wrapping

The general procedures of FBP-1 synthesis, protein expression and purification, and protein wrapping procedure were same with Chapter 2. The only difference was that the functional amino acid propargylglycine was added at the ninth position of the sequence in Figure 3.3.

3.2.3 Polysulfone modification

- Chloromethylation of PSU

10 grams of PSU was dissolved in 300 mL chloroform in a 500 mL round bottom flask under argon atmosphere. 6.7 g Paraformaldehyde, 0.26 mL $SnCl_4$ and 28.5 mL $(CH_3)_3SiCl$ were added into the reaction flask, respectively. The mixture was stirred at 60 ^oC for 72 hours. The reaction formula was shown as the first step of figure 3.4. After reacting 72 hours, the polymer solution was precipitated in methanol and washed several times with methanol. Polysulfone chloride (PSU-Cl) was then filtered and dried under vacuum [89].

- Azidation of PSU

1 gram of above obtained PSU-Cl was dissolved in 15 mL of DMF in a round-bottom flask. 0.097 gram of Sodium azide was added to the solution. The mixture solution was stirred for 24 hours at 70 ^oC. After 24 hours, the reaction mixture was concentrated and precipitated into methanol/water mixture (v/v: 4/1). The product polysulfone azide (PSU-N_3) was dried in a

vacuum at 25 ºC[90].

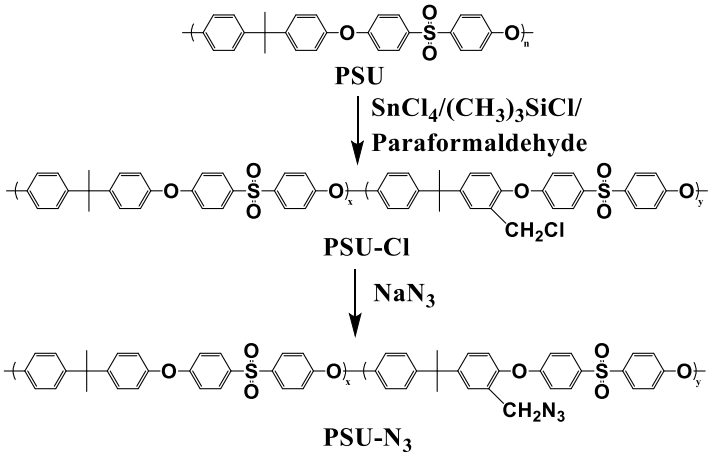

Figure 3.4 Overall process for the modification of azide functionalized polysulfone (the first step: Chloromethylation of PSU; the second step: Azidation of PSU).

3.2.4 Functional substrate casting

The porous PSU-N_3 membrane was prepared by the liquid-induced phase inversion technique. The casting polymer solution was prepared by adding 12 wt% of PSU, 8% of PSU-N_3 into NMP at 70 ◦C. After polymer dissolved, PVP was blended in as the pore-forming agent at a concentration of 7 wt%. The viscous solution was then filtered through a coarse glass fiber filter and degassed under vacuum. The filtered solution was casted onto a glass plate, which was then immersed in DI water at 25 ◦C. After the membrane had detached from the glass plate, it was kept in another water bath for at least 24 h[91].

3.2.5 Click chemistry

For a click reaction between AqpZ/FBP-1 complex and PSU-N_3 substrate(Figure 3.5a),

100 μM $CuSO_4$, 2 mg AqpZ/FBP-1 and 500 μM ligand PMDETA were mixed with 10 mM NaH_2PO_4 buffer in a schlenk flask. The mixed solution was purged with N_2 for 30 min and then forced circulate through PSU-N_3 membrane by peristaltic pump (Figure 3.5b). In the same time 2.5 mM sodium ascorbate was added into the circulate system. The reaction system was sealed for 24 hours. The obtained PSU-AqpZ membrane was washed by DI water for several times and kept in water at 4 °C.

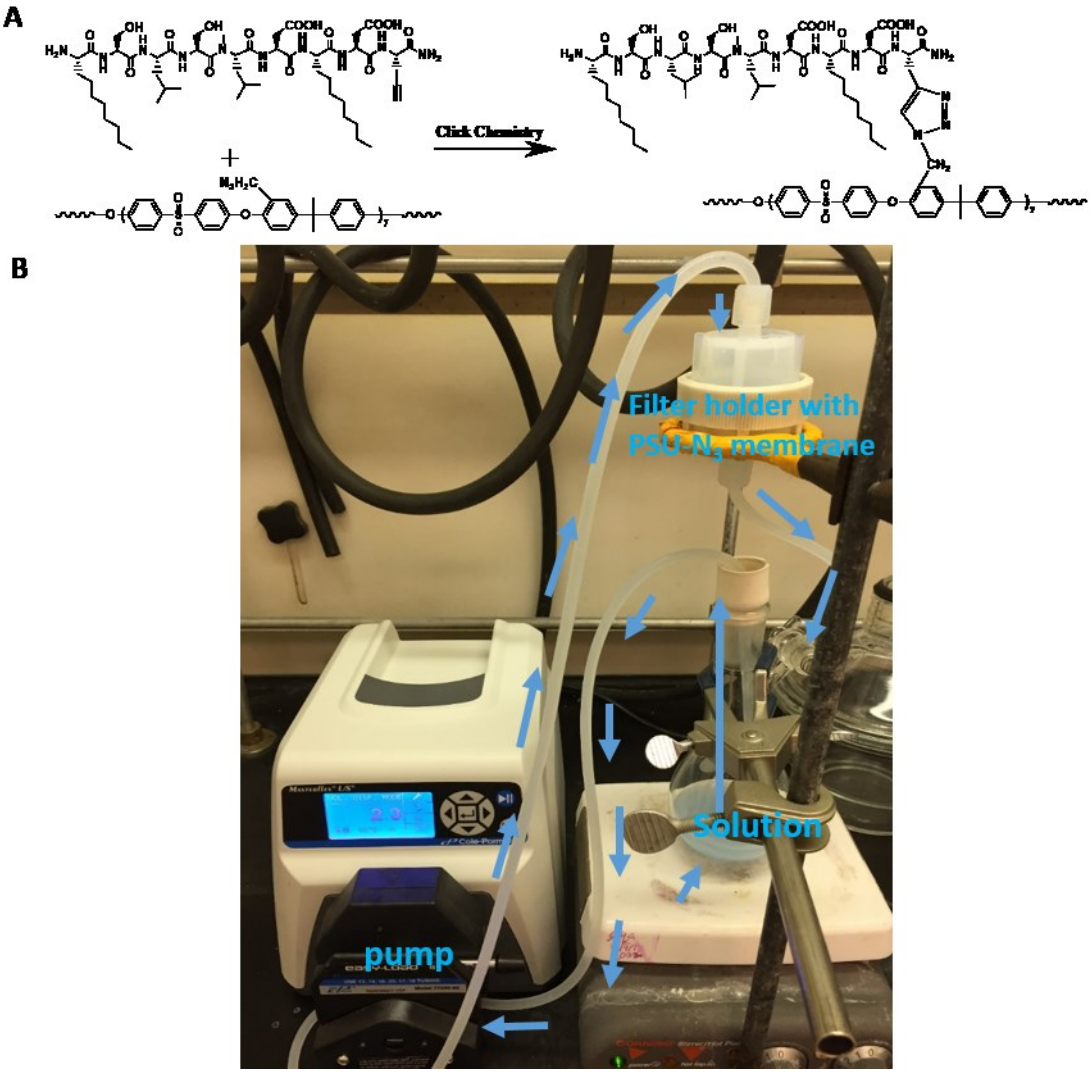

Figure 3.5(a) The click conjugation between FBP-1 and PSU-N_3; (b) The click reaction set up (there parts were included: peristaltic pump, membrane with filter holder as support, and reagent solution. The blue arrows indicate the circulation direction).

3.2.6 Characterizations

- **Characterizations of FBP-1 and AqpZ/FBP-1 complex**

Jasco J-810 CD Spectropolarimeter (Jasco, Japan) was utilized to investigate the secondary structures of FBP-1, AqpZ and AqpZ/BP-1 complex. Similar to chapter 2, samples were all prepared in 10 mM NaH_2PO_4 buffer with pH 7.4. The CD experiments were performed under scanning wavelength from 190 nm to 260 nm with1.0 nm step, 1.0 nm bandwidth and a 3s collection time per step at 25ºC in a 0.1 cm pathlength quartz cell.

- **Characterization of FBP-1 functional group**

To determine the alkyne functionality of FBP-1, one fluorescence dye was clicked with FBP-1. Subsequently, the emission scan of the product was obtained by a PTI Fluorescence Spectrophotometer (Photon Technology International, Lawrenceville, NJ, USA). The excitation wavelength was set at 535 nm and recording emission signal from 565 nm to 700 nm.

- **Characterization of polymer modification**

^{1}H NMR measurements were recorded using Varian Direct Drive VNMRS 600 spectrometer (Agilent Technologies, Santa Clara CA) operating at a magnetic field strength of 14.1 T (600 MHz 1H frequency) using Chloroform-d ($CDCl_3$) solvent. Measurements were acquired at R.T. using a single pulse excitation with a 45º flip angle of 3.6 µs. Acquisition time

was maintained at 1.7 s with repetition time one second. PSU, PSU-Cl, and PSU-N_3 spectra were recorded separately.

- **Characterizations of membrane surface composition**

FTS 7000 FTIR spectrometer (Varian Inc., Palo Alto, CA, USA) equipped with ATR set up was used to analyze the characteristic function groups on sample membranes. Membrane samples were first dried under vacuum for overnight at 25 ºC. The transmittance spectra were recorded with a spectral resolution of 4 cm^{-1}. XPS analysis was also conducted to analyze the surface chemical element composition by using AXIS 165 XPS Spectrometer. All the bonding energies have been corrected by referring to the C 1s photoelectron peak at 284.6 eV. Membrane samples of PSU, PSU-N_3 and PSU- AqpZ were tested and recorded. Image Quant LAS 4000 biomolecular imager (GE healthcare, United Kingdom) was utilized for detecting fluorescein on the membrane surfaces. Images of membrane samples were taken at Fluorescence mode via blue epi-illuminator to excite fluorescein.

- **Characterizations of surface morphology of membranes**

Zeiss Sigma Field Emission Electron Microscope (Zeiss, Germany) was used to observe the morphology of membranes. To prepare the SEM sample, the membrane was dried under vacuum overnight at 25ºC and coated with a ~5 nm thick gold to minimize the charging effect. Observation was performed under 5 kV and in-lens state. Zeiss Orion Helium Ion Microscope was applied to directly image membrane samples without coating any gold on the surface. Membrane samples of PSU and PSU-AqpZ were scanned to analyze the original surface morphology.

3.2.7 Preliminary desalination performance test

Desalination properties of the synthesized biomimetic membranes were characterized in the same cross flow reverse osmosis setup as chapter 2. Differently, membranes were tested at 50 PSI in order to protect the membrane delicate structure and get reasonable water flux and rejection values. Similarly, the water flux (J_w) was calculated from collected permeate volume at a unit time on a unit membrane area ($(\frac{\text{Liter}}{m^2 \times hour})$, LMH).And the salt rejection (R) was obtained based on the conductivity differences between the feed solution and the permeate solution by conductivity meter (inlab 741, mettle toledo), ($R = 1 - C_p/C_f$).

3.3 Result and discussion

3.3.1 Polymer characterizations

The high functionalization degree of PSU-N_3 was required for better bio-conjugation to load AqpZ/FBP-1 complex onto the resulting functional substrate. Figure 3.6c shows the ^1H NMR spectra of PSU-Cl and PSU-N_3 in $CDCl_3$. From the red line spectrum in Figure 3.6c, the peak at 4.53 ppm was assigned to the methylene of the CH_2Cl group (denoted as *a* in Figure 3.7c). The peak at 7.83 ppm was assigned to the four meta protons on the phenyl ring adjacent to the sulfonyl group (denoted as *b* in figure 3.6c). The degree of chloromethylation was calculated to be around 1.25 Cl per repeating unit of PSU from the intensity ratio of these two types of peaks[92].

The blue line in Figure 3.6c shows the ^1H NMR spectrum of PSU-N_3 in $CDCl_3$. Compared with the spectrum of PSU-Cl, the signals corresponding to methylene protons shifted from 4.53

ppm to 4.37 ppm(denoted as *c* in Figure 3.6c), and the peak intensity at 4.53 ppm was decreased (denoted as *a'* in Figure 3.6c). This result indicated the successful azidation reaction. The conversion rate of CH_2Cl to CH_2N_3 was calculated to be 84% from the intensity ratio between *c* and *a*. The average azide group density on the PSU chain was calculated to be ~1.05 N_3 per repeating unit of PSU. From the result, each unit of polysulfone was attached by at least one azide group, which was favorable for the subsequent click reaction between the substrate and AqpZ/FBP-1 complex.

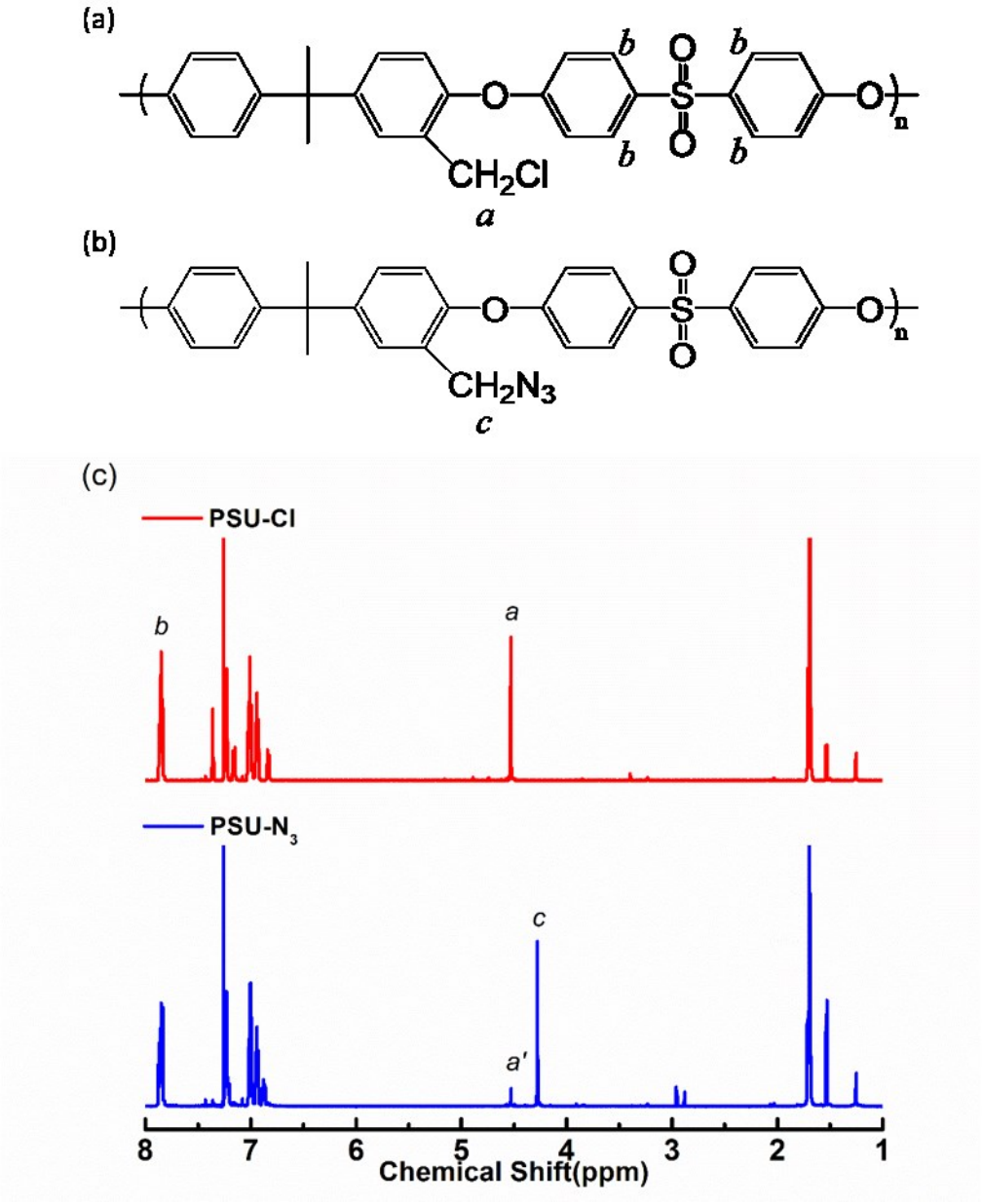

Figure 3.6(a) Chemical structure of PSU-Cl. *a* and *b* indicate the different types of characteristic signal peaks used to calculate the degree of chloromethylation according to ^{1}H NMR spectrum of PSU-Cl. (b) Chemical structure of PSU-N_3. *c* represents the new peak appeared in its ^{1}H NMR spectrum.(c) ^{1}H NMR spectra of PSU-Cl (red line) and PSU-N_3 (blue line).

3.3.2 Characterizations of FBP-1

- **The secondary structure of FBP-1**

The identity of purified FBP-1 was verified by ESI-MS. Two main peaks were observed: m/z 1135.82 (1135.66 calcd for $[FBP\text{-}1\text{-}H^+]^-$) and m/z 1157.80 (1157.64 calcd for $[FBP\text{-}1+Na^+\text{-}2H^+]^-$). The secondary structure of FBP-1 in aqueous solution was studied by circular dichroism analysis, as shown in Figure 3.7. A characteristic β-sheet signal at 218 nm was observed from CD spectrum of FBP-1, which suggests the formation of β-sheet secondary structure of FBP-1 in aqueous solution. Therefore, adding propargyl group into the sequence does not affect the β-sheet formatting ability in BP-1. FBP-1 still has the capability to self-assemble into β-sheet structure in aqueous solution.

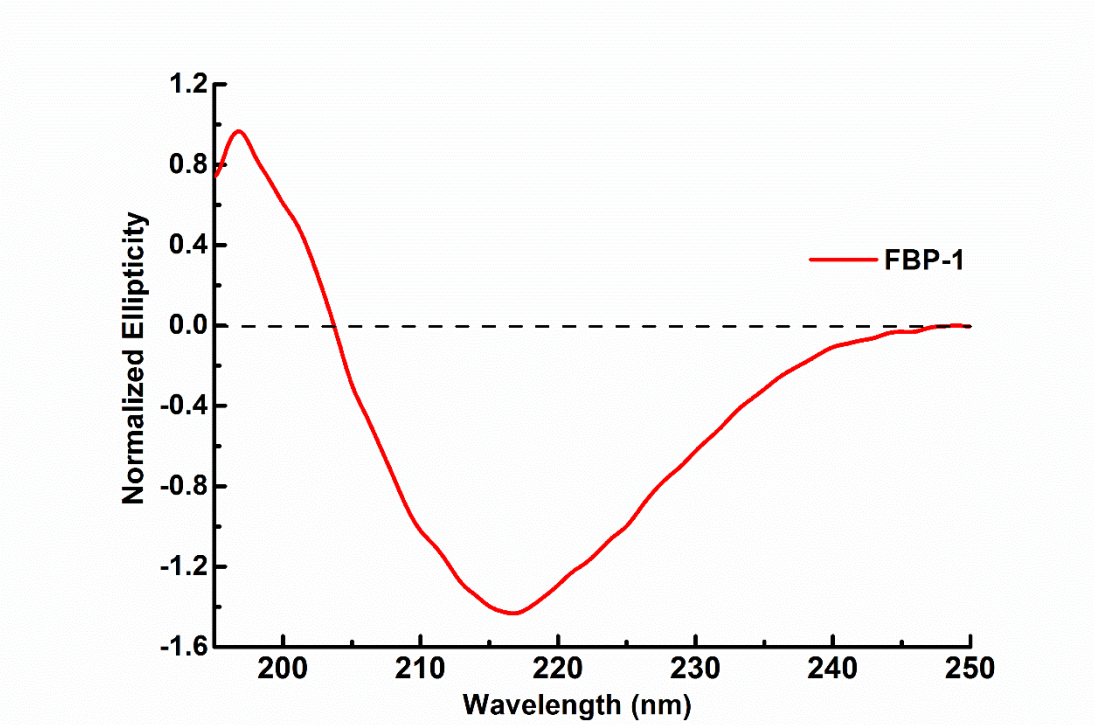

Figure 3.7 Circular dichroism spectrum of FBP-1.

- **The functional end of FBP-1**

Red fluorescent dye TAMRA-azide (Ex/Em 555/580 nm) and Click-iT® protein reaction buffer kit was used to demonstrate the functionality of the propargyl group of FBP-1. Click reaction was performed following the manufacturer's instruction to conjugate TAMRA-azide to FBP-1 resin (Figure 3.8). After washing out remaining dye residues and cleaving FBP-1 from the resin, FBP-1 was recrystallized in ether and dissolved again in DI water for fluorescence spectroscopy characterization.

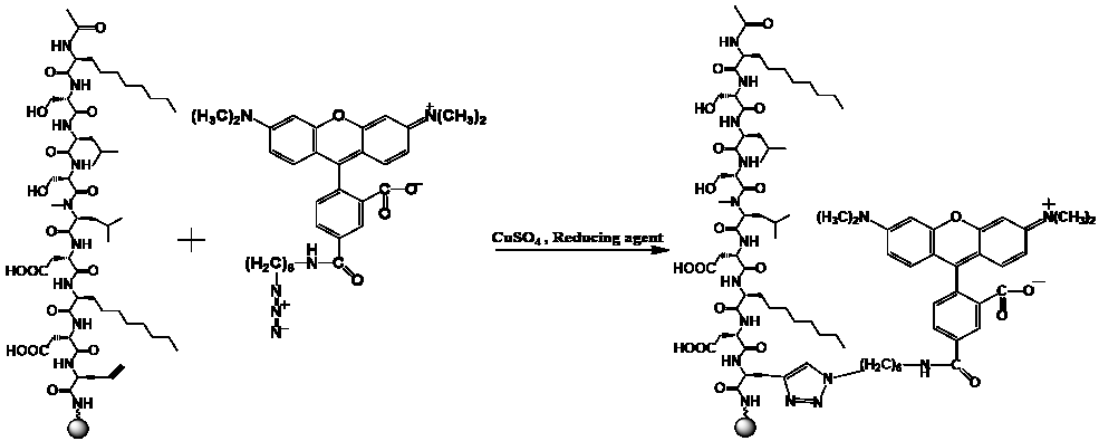

Figure 3.8 The reaction formula of Red-fluorescent TAMRA-azide reacting with FBP-1 before cleavage.

The emission scan of the product was shown in Figure 3.9. The fluorescence emission peak at 575 nm was obtained when applied an excitation light with wavelength of 535 nm, which indicates that FBP-1 was successfully clicked with TAMRA-azide dye. Therefore, FBP-1 functional alkyne end has the capability to react with azide functional chemicals via click

chemistry.

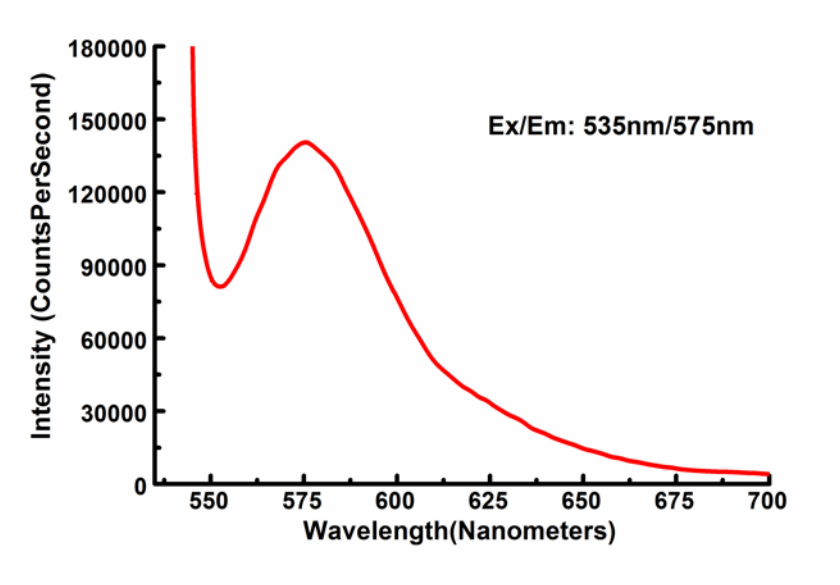

Figure 3.9 Fluorescence emission spectrum for the product of FBP-1 click with TAMRA-azide. An excitation with wavelength of 535 nm was applied and an emission peak at 575 nm was observed.

3.3.3 Stability study of AqpZ/FBP-1 complex

The stability of AqpZ and FBP-1 complex was characterized by CD after removing DDM via dialysis. As shown in Figure 3.10, AqpZ/FBP-1 complex (in red) still maintained alpha-helix structure of AqpZ with typical alpha-helix ellipticity signal at 193 nm, 210 nm and 221 nm[72]. However, the control sample (in black) without adding FBP-1 lost the predominant alpha-helix structure, which indicates that the AqpZ was partly denatured after same dialysis procedure. It demonstrates that FBP-1 is able to substitute detergent and stabilize AqpZ in aqueous solution. In addition, it proves that the functional end propargyl group does not influence the wrapping process around the protein.

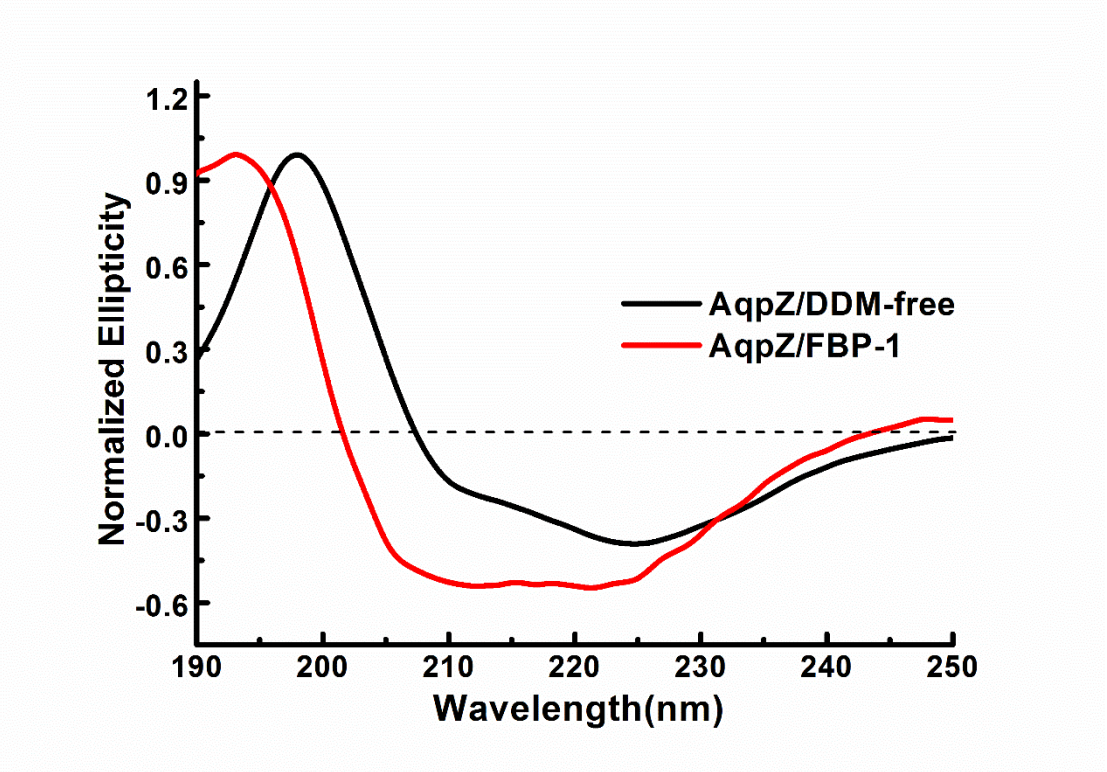

Figure 3.10 CD spectra of AqpZ/DDM-free (black line), and AqpZ/FBP-1 (red line) after dialysis.

3.3.4 Chemical compositions of the conjugated PSU-AqpZ membrane surfaces

ATR was utilized to characterize and compare the chemical compositions of the surfaces of PSU-N_3 and the membrane after click reaction with AqpZ/FBP-1 complex (PSU-AqpZ membrane). As shown in Figure 3.11a, the IR adsorption at 2098 cm^{-1} in the spectrum of PSU-N_3 bands (black line) is corresponding to azide groups. The IR signals at 3302 cm^{-1} and 1660 cm^{-1} are derived from NH stretching and C=O stretching vibrations of amide group[93], which indicates the presence of protein structure. Further compare the two spectra in region of 2350 cm^{-1} to 1350 cm^{-1}(Figure 3.11b), the azide signal at 2098 cm^{-1} was slightly decreased after click

reaction, and one new peak generated at 1543 cm^{-1} which was agreed with the literature value for a 1,2,3-triazole[94, 95]. As a result, the conjugation reaction occurred successfully between AqpZ/FBP-1 complex and azide substrate. In addition, as the penetration depth of ATR into the sample is typically between 0.5 and 2 micrometers[96], the azide group from bulk PSU-N_3 under surface is still detectable, which explains the existence of azide signal in PSU-AqpZ membrane IR spectrum.

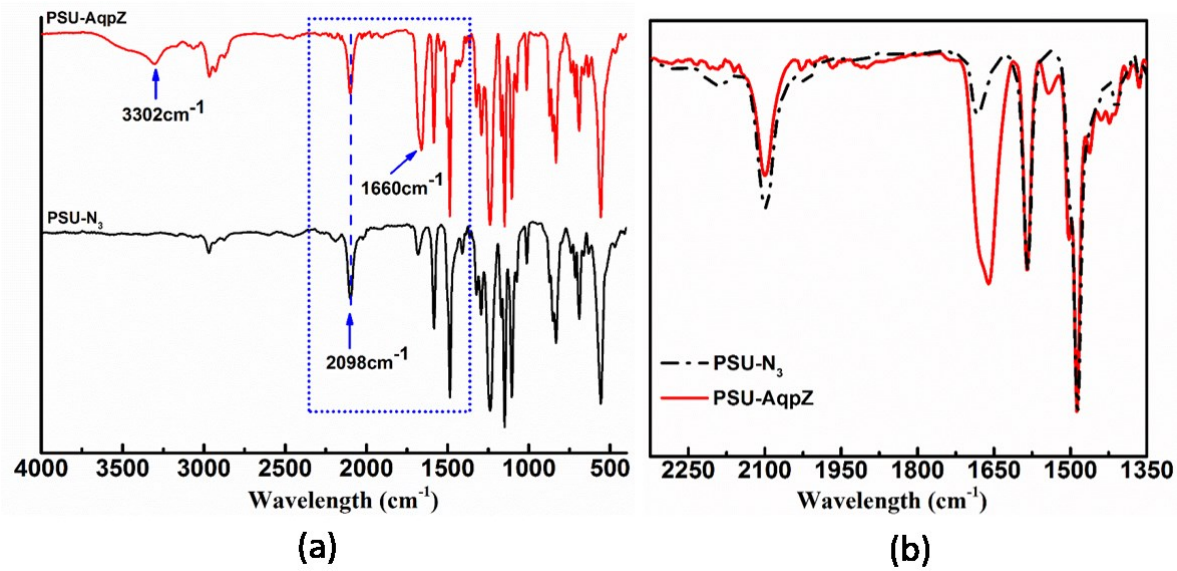

Figure 3.11(a) ATR spectra of PSU-AqpZ membrane (red line) and PSU-N_3 membrane (black line); (b) IR difference spectra of PSU-AqpZ membrane (red line) and PSU-N_3 membrane (black dash) from 2350 cm^{-1} to 1350 cm^{-1}, according to the blue dot region in (a).

The membrane surface chemical composition was also characterized by XPS analysis (Figure 3.12). All the wide scan spectra have the same distribution of peaks, including the peak at 532 eV assigned to O 1s, 285 eV assigned to C 1s, 399 eV assigned to N 1s, and 168 eV assigned to S 2p[97]. The corresponding composition of both membrane surfaces is listed in Table 3.1. The nitrogen component from PSU membrane is resulted from the pore agent PVP

added during the substrate casting procedure. Thus for PSU membrane surface, the N1s core level spectrum only presents one peak with binding energy at 399.5eV, which is contributed by the nitrogen in PVP[97, 98]. Compared to PSU membrane, PSU-N_3 membrane shows higher N/S content ratio due to successful azidation modification of PSU. The increase of the N/S content ratio after click reaction is resulted from the relatively higher nitrogen content of AqpZ, which indicates the successful tethering of AqpZ/FBP-1 complex on the membrane surface. For PSU-N_3 surface, N 1s core level spectrum is curve-fitted into four peak components with binding energies at 404.2, 400.7, 399.9, and 399.6 eV, attributable to the (C)−N=, N^-, N^+, and the nitrogen from PVP respectively[97, 99]. For PSU-AqpZ membrane, the broad N 1s peak can be fitted and deconvoluted into five peaks with the following tentative assignments: 404.2(the residual N^+ from azide group), 401.0(-C-N- from triazole ring), 400.5(N=N from triazole ring), 400.0(nitrogen from amide group), 399.5(the nitrogen from PVP) and 398.8 eV(nitrogen from amine group)[97, 100-102]. The depressed peak of N+, and the presence of new peaks indicate that the amount of aizde group on the surface was relatively decreased and AqpZ/FBP-1 complex was conjugated on the surface.

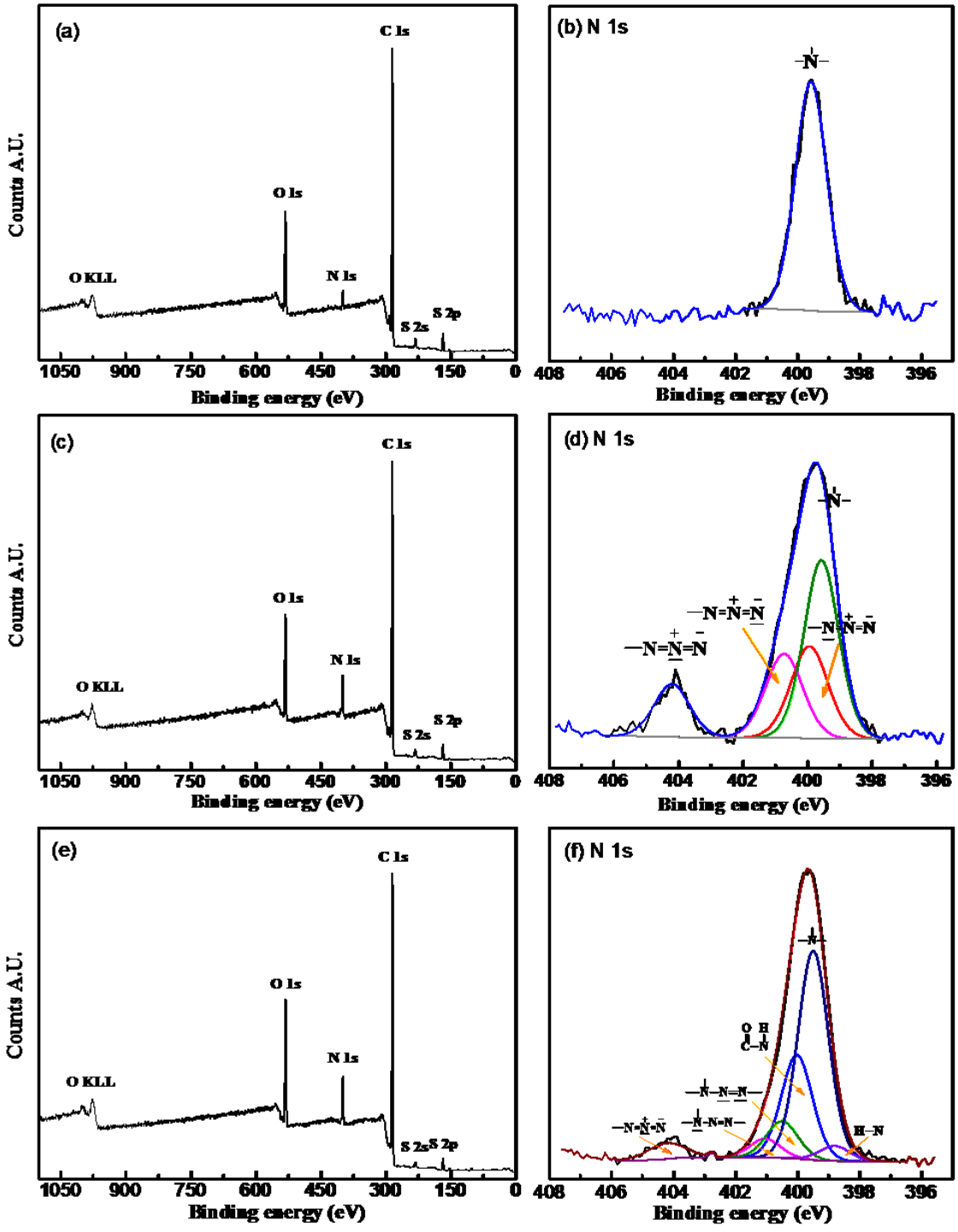

Figure 3.12 Wide scan and N 1s core level XPS spectra of PSU membrane surface (a and b),

PSU-N_3 membrane (c and d), and PSU-AqpZ membrane surface (e and f).

Table 3.1 Chemical compositions of the PSU, PSU-N_3 and PSU-AqpZ membranes by XPS.

Membrane Sample	C 1s [mol%]	O 1s [mol%]	N 1s [mol%]	S 2p [mol%]	n(N)/n(S) [mol/mol]
PSU	82.59	12.02	2.28	3.10	0.735
PSU-N_3	79.29	11.30	7.17	2.24	3.2
PSU-AqpZ	78.61	12.62	6.85	1.92	3.57

3.3.5 Florescence study to confirm the conjugation between AqpZ complex and functional substrate

For observation purpose, fluorescein isothiocyanate (FITC), one synthetic organic compound was chosen as a fluorescent tracer for AqpZ. It has an absorption maximum at 494 nm and emission maximum of 512 nm in aqueous solution. Briefly, the isothiocyanate group of FITC was able to react with the primary amine groups of AqpZ and form a thiourea linkage. Consequently, the labeled AqpZ is detectable by fluorescence spectroscopy, which makes the FITC labeling an effective method to determine the presence of AqpZ. In order to further demonstrate that the AqpZ/FBP-1 complex was conjugated on membrane surface via click chemistry, rather than non specific binding, same amount of FITC-AqpZ was wrapped by FBP-1 and BP-1 respectively. Two click reactions were carried out by using FITC-AqpZ/FBP-1 and FITC-AqpZ/BP-1 complex (Table 3.2). After click reaction, both M1 and M2 was washed in DI water thoroughly to get rid of non-binding protein on the surface. Membranes were then characterized by gel document imaging system.

Table 3.2 Click reaction conditions for fabricating membrane M1 and membrane M2.

Sample ID	Click reaction conditions
M1	2 mg FITC-AqpZ/BP-1 100 μM $CuSO_4$ 500 μM ligand PMDETA 2.5 mM sodium ascorbate
M2	2 mg FITC-AqpZ/FBP-1 100 μM $CuSO_4$ 500 μM ligand PMDETA 2.5 mM sodium ascorbate

During the preparing procedure, the only difference between two membranes is the wrapping peptide—M2 using the peptide with alkyne group which is clickable with the azide surface, and M1 using the peptide without any functional group to react with the surface. Figure 3.13 shows the results of M1 and M2 from gel document imaging machine. As shown in Figure 3.13a, no FITC signal is observed for M1 surface, indicating no FITC-AqpZ is bound to the surface. Compared to M1, strong green fluorescence is observed from M2 surface, which suggests that FITC-AqpZ was anchored onto the membrane surface. Therefore, the fluorescence result reveals that the AqpZ/FBP-1 complex was conjugated onto the surface via click reaction between FBP-1 and azide surface. This also proved that the intermolecular force between FBP-1 and AqpZ was relatively strong and able to maintain the complex during click reaction.

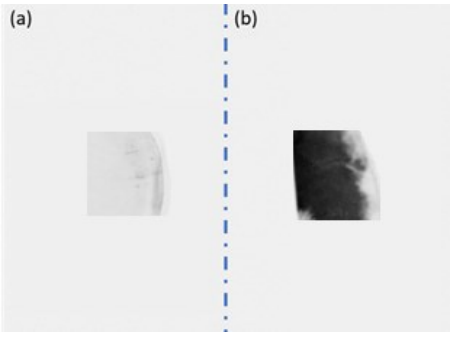

Figure 3.13 Fluorescence image of (a) M, (control membrane for click reaction by using BP-1

as wrapping agent); and (b) M2, (click membrane using FBP-1 as wrapping agent). Images taken by gel document imaging system at excitation of 490 nm and the black area represents the emission signal at 525 nm.

3.3.6 Morphology study of the PSU-AqpZ membrane surfaces

The surface morphology was first characterized by SEM (Figure 3.14). The top surface of the PSU-N_3 substrate is smooth and no pore structure was observed under low magnification (Figure 3.14a). Under high magnification, small pores were able to be observed with the size around 8 nm, which indicates that the substrate has a tight structure with appropriate size of pores for protein complex (Figure 3.14b). For the cross-section image, the membrane presents asymmetric structure, which consist of a dense skin layer (Figure 3.14d between the red arrows) and a porous sublayer having a fingerlike structure (figure 3.14c). This is a typical structure for membranes prepared from liquid-induced phase inversion[88]. During the click reaction, the reaction solution including reaction reagents and AqpZ/FBP-1 complex were filtered and circulated from top dense layer to bottom. As shown in Figure 3.14e, the PSU-AqpZ membrane surface is relatively rougher and covered uniformly by tight and small nodular spots with the size around 25 nm, compared to PSU-N_3 membrane surface. Nevertheless, the SEM samples were coated by 5 nm thick gold, which may influence the surface morphology.

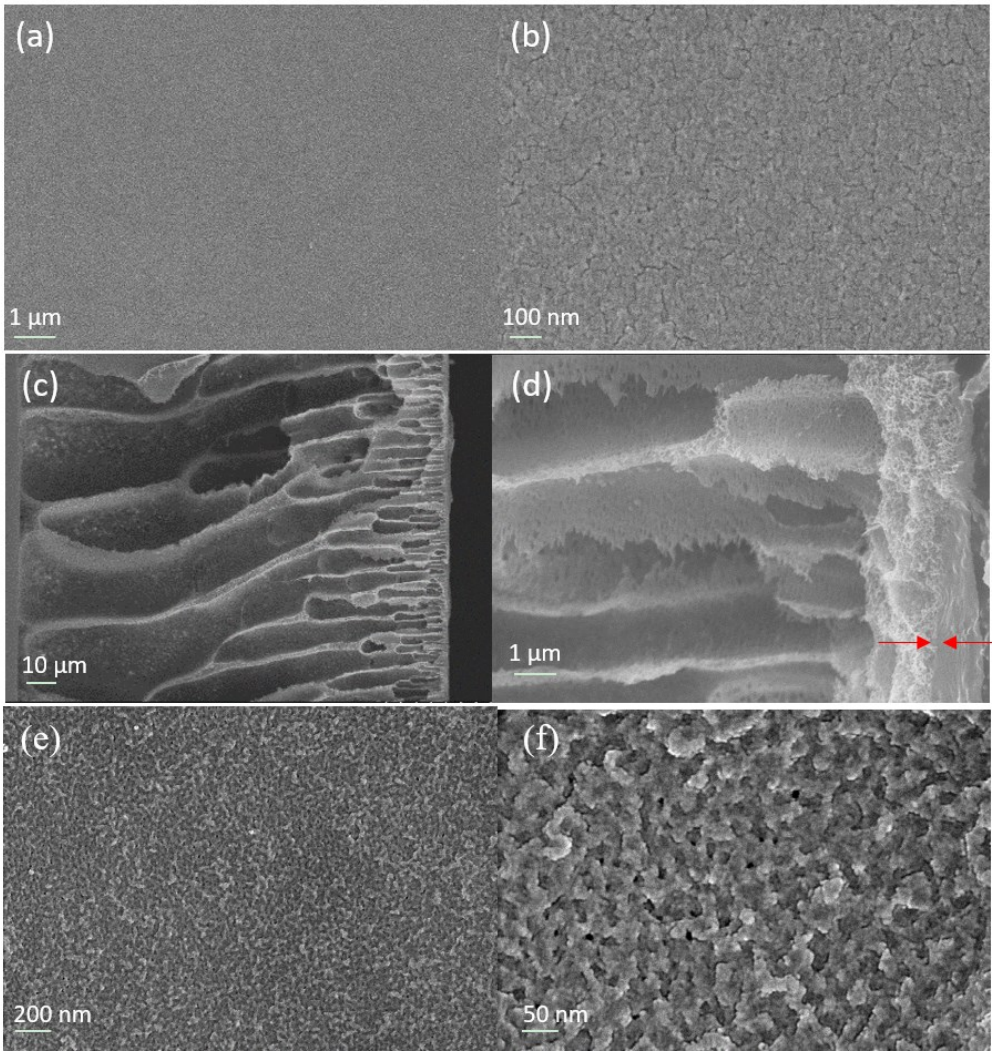

Figure 3.14 SEM images of the membrane surfaces. (a)Top view of PSU-N_3 membrane; (b) Top view of PSU-N_3 membrane surface in high resolution; (c) Cross-section view of PSU-N_3 substrate; (d) High resolution image of the cross-section of PSU-N_3 substrate, the red arrows in (d) denoted the dense layer of PSU-N_3; (e) Low resolution image of PSU-AqpZ membrane surface; (f), High resolution image of PSU-AqpZ membrane surface; all the samples were gold coated).

In order to further confirm the conjugation of the complex on the surface, we tried to use HIM to image the PSU-AqpZ membrane (Figure 3.15). HIM is an imaging technology based on

using a scanning helium ion beam rather than the electron beam, which gives an advantage of directly characterizing non-conductive samples without any charging effect[103]. Therefore, no coating is required and HIM images of non-coated samples are more close to the reality of the surface morphology compared to SEM images of gold coated samples. Figure 3.15a exhibits the smooth surface of PSU-N_3 membrane and small pores were observed from the image. Compared with PSU-N_3 membrane, the surface of PSU-AqpZ membrane (Figure 3.15b) was covered by AqpZ clusters (white spots). Similar to SEM result, dense sphere-like small bumps with the size approximately around 25-35 nm were observed on the surface (figure 3.15c). Nevertheless, the edge contrast is lower compared to SEM images, resulting from high energy rigid helium ion beam struck on the soft protein sample and might mill the surface structure of the sample[104].

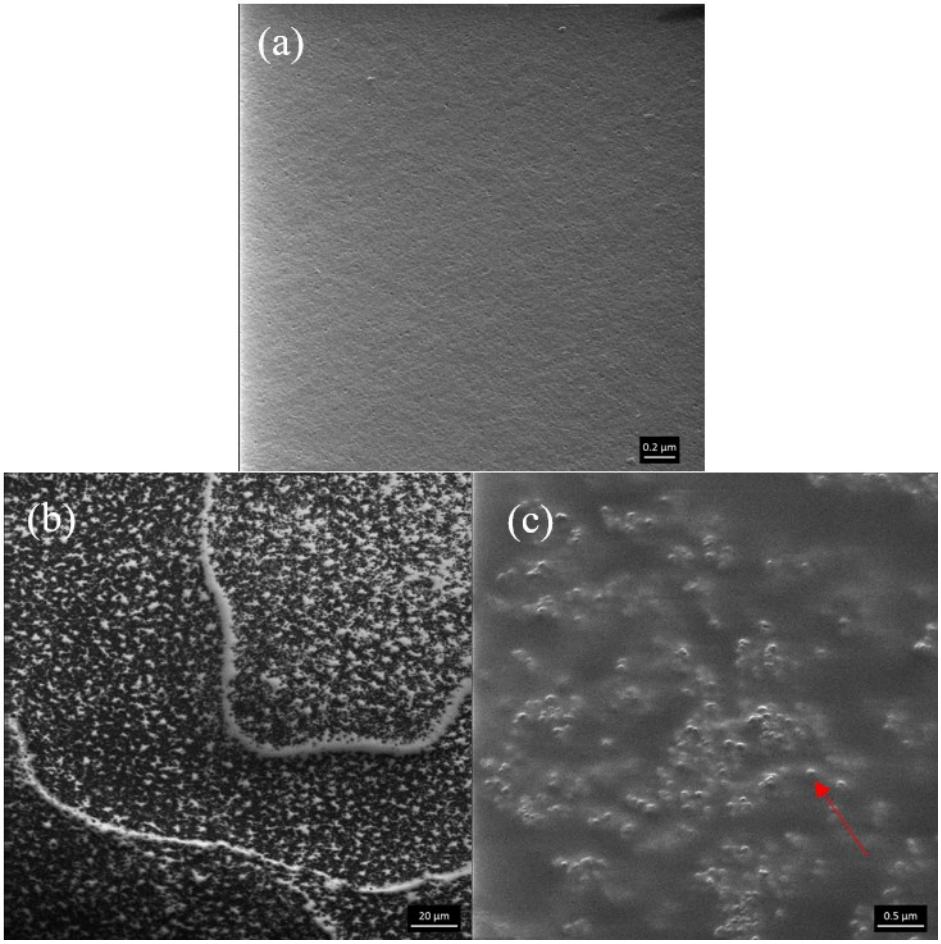

Figure 3.15 HiM images of (a) PSU-N_3 membrane, (b) and (c) PSU-AqpZ membrane. The red arrow was pointed at one bump structure on the membrane. all samples were non-gold coated.(Images were obtained by Peng Li)

As the dimension of tetramer AqpZ is about 6 nm × 6 nm × 6 nm [105, 106], the length of AqpZ/FBP-1 complex should be slightly larger than 6nm. This suggests that the small sphere structure could be resulted from the presence of AqpZ/FBP-1 complex on the top of the membrane. Based on the result of the SEM and HIM imaging, it appears that AqpZ is successfully anchored on the surface but in a clustered manner, with approximate 4 molecules of the AqpZ monomer in each cluster. The cluster might happen at varied steps during the whole

procedure, for example, it could happen before the conjugation such as during the protein-peptide complex formation, or it could happen during the conjugation step. The specific cause remains to be investigated. Nonetheless, it is verified that the FBP-1 can mediate the conjugation of AqpZ onto polymeric functional membrane substrate while protect protein from denature.

3.3.7 Preliminary test of desalination performance

The desalination performances of PSU-N_3 and PSU-AqpZ membranes were carried out on cross-flow machine at 50 PSI using 1 g/L NaCl feed solution at 25 ºC. The results were recorded in Table 3.3. The water flux decreased and salt rejection increased after click AqpZ/FBP-1 complex clicked on the surface. As a circulating solution was applied during click reaction, theoretically, AqpZ/FBP-1 complex was trapped and reacted inside or around the nano-size pores of the substrate. Therefore, part of the pores on the substrate surface was covered with the complex, which slows molecules passing through the membrane. This explains the depressed water flux and slightly higher salt rejection.

Table 3.3 Preliminary water performance test of PSU-N_3 and PSU-AqpZ membranes

	PSU-N3 membrane	PSU-AqpZ membrane
Water flux (LMH)	17.13±1.87	4.53±2.33
Salt rejection (%)	5%	12.5±4.2%

- Tested at 50PSI using 1g/L NaCl feed solution with concentrate flow 0.6 GPM at 25 ºC.

The idea of clicking AqpZ/FBP-1 complex onto the surface under circulate condition was aimed to lead the click reaction happen around the pore or inside the pore. Hypothetically, pores on the substrate were filled by AqpZ/FBP-1 complex after the reaction. Since AqpZ only allows water molecules to pass though, the membrane will display enhanced salt rejection. The results

shows a moderate improve of salt rejection (from 5% to 12 %). The suboptimal salt rejection (12%) of the PSA-AqpZ membrane suggests that there are defects on the membrane. As shown in Figure 3.16a, the ideal situations for locating AqpZ/FBP-1 complex are the AqpZ clicked straight upon a similar size pore on the surface, or several complex packed and clicked around a bigger size pore to block it. However, some AqpZ/FBP-1 complex may dislocate and fail to fully cover the pore (Figure 3.16b), which lead to leaking of salt ion passage and low salt rejection of the membrane. Therefore, the defects from low degree of click conjugation directly upon the pores (including not fully filling up the pores) resulted in the low salt rejection of PSU-AqpZ membrane.

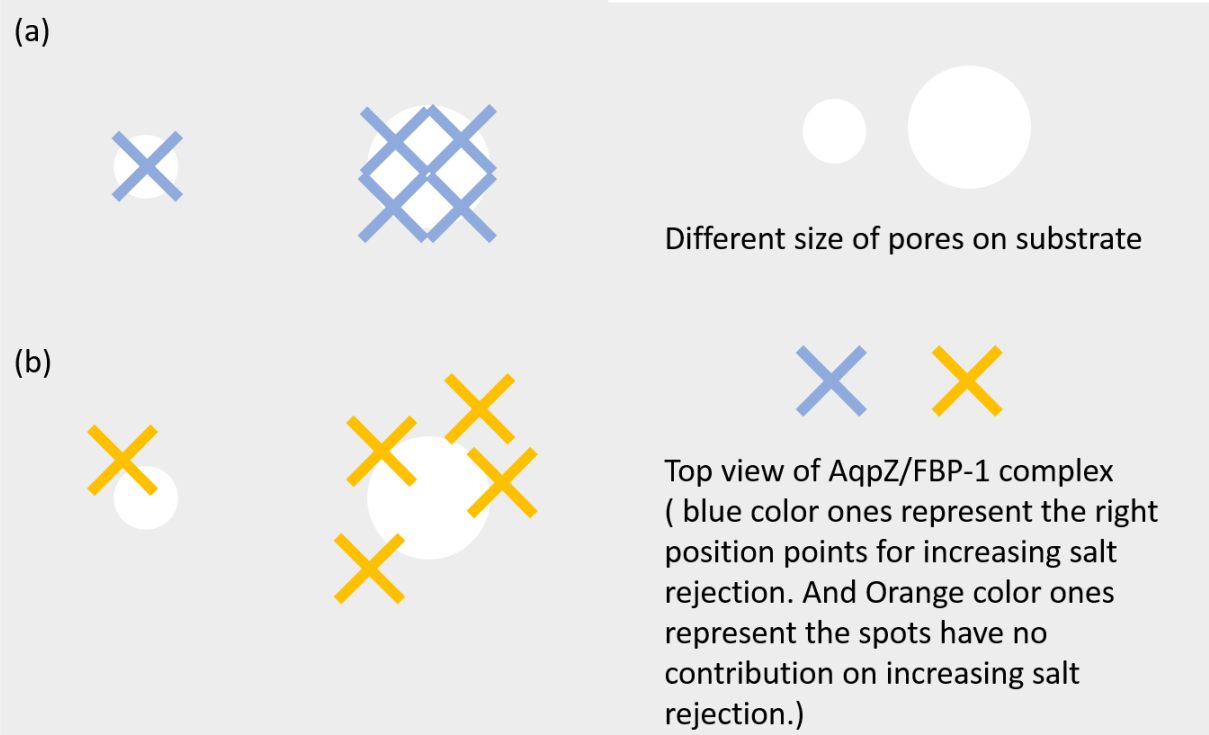

Figure 3.16 Cartoon scheme of the possible location and position of AqpZ/FBP-1 complex clicked on the surface.

3.4 Conclusion

In this chapter, the fabrication of a novel biomimetic membrane by conjugating AqpZ/FBP-1 complex on functionalized substrate, and its desalination performance were investigated. Given the advantages as bio-inert, compatible with aqueous media and high yield, click chemistry was chosen as the method to incorporate AqpZ into membrane system to fabricate the desalination biomimetic membrane. Peptide with alkyne group was successfully synthesized and the activity of functional group was verified. Polysulfone, chosen as the starting substrate polymer material was modified with azide functional group. AqpZ was successfully stabilized by FBP-1 and the complex was proved to be clicked on the substrate. However, the salt rejection and water flux of the obtained membrane only improve moderately compare to the control sample. This suggests that the current reaction strategy is not able to fill up the pore space in the substrate with AqpZ/FBP1 complex. Future work on minimizing open pores defects to increase salt rejection can be performed to fabricate qualified desalination membranes.

Chapter 4. Conclusions and future work

4.1 Conclusions

In this thesis, amphiphilic peptides were utilized as a novel tool to stabilize water channel protein AqpZ. BP-1 was first demonstrated to have excellent ability to tightly bind with AqpZ by hydrophobic force and further form β-barrel around the protein by intermolecular hydrogen bonding with each other, resulting in stable AqpZ/BP-1 complex in aqueous solution. Meanwhile, the solid chemistry synthesis of peptide offered an easy and favorable way to modify the peptide with functional groups. Functional peptide FBP-1 with alkynyl group was successfully synthesized by adding propargyl glycine into peptide sequence. The resulting FBP-1 thus exhibited dual functions: (1) stabilizes AqpZ in aqueous solution; and (2) serves as a linker to conjugate AqpZ to polymeric substrate.

Two strategies were developed in this work to incorporate stable AqpZ complex into membrane system for fabrication of robust biomimetic desalination membranes. AqpZ/BP-1 complex was successfully encapsulated into a dense polyamide barrier layer via interfacial polymerization on a polysulfone substrate. The resulting composite membrane showed enhancement of water permeability while maintaining high salt rejection over the testing time. Meanwhile, the membrane exhibited robust mechanical stability, evidenced from its tolerance of high testing pressure. No defects were formed during the fabrication process and the polyamide layer protected the complex from peeling off. This study clearly demonstrated the promising potential of preparing high performance biomimetic membranes by incorporating AqpZ/BP-1 complex into interfacial polymerization.

The effect of the complex adding amount on membrane desalination performance was also investigated in this study. Although the water permeability was increased linearly in low adding amount, it reached maximum when the surface reached the saturate absorption of AqpZ/BP-1 complex. To further improve the water permeability, covalent binding between the complex and surface, instead of the non-specific van der Waals interaction, may be required.

Another strategy to fabricate biomimetic desalination membrane studied in this thesis is to conjugate AqpZ/FBP-1 complex onto the porous azide substrate via mild click chemistry. Polysulfone was chosen to be the starting material for substrate and was first modified with azide group. The consequent polysulfone azide was then casted using liquid induced phase separation technique, resulting in a thin film substrate with appropriate pore size structure. Click reaction was performed using circulating system. The consequent membrane revealed that the functional complex was successfully conjugated onto the membrane surface as supported by surface chemical composition analysis (XPS, FTIR etc.). This study reveals a promising and universal method to conjugate a thin layer of proteins onto polymeric substrate. However, defects exist as pores were not fully covered by AqpZ/FBP-1 complex, resulting in low salt rejection of the consequent membrane.

4.2 Future work

In summary, two novel methods of incorporating water channel protein AqpZ to fabricate biomimetic desalination membranes reveal great potentials in future desalination industry practice. To fabricate ideal biomimetic desalination membranes, future work and improvement shall be focus on as following:

In chapter 2, to find out the saturate point of the AqpZ complex amount on the membrane, the exact AqpZ complex loading amount needs to be quantified. The protein amount can be detected on the membrane surface after interfacial polymerization, or can be calculated by quantifying the amount of protein in the extra aqueous phase. The latter approach is more technically practical. To quantify the AqpZ complex amount in the extra aqueous phase, accurate method for detecting low concentration of protein is required. Given that the expected protein concentration in the extra aqueous phase would be under 3 μg/mL, the bicinchoninic acid assay (BCA assay) and fluorescence assay (using NanoOrange Protein Quantitation Kit) are both suitable for the protein quantification here. Both assays have high sensitivity (0.5 μg/mL to 1.5 mg/mL for BCA assay, and 10 ng/mL to 10 μg/mL for fluorescence assay)[107]. The AqpZ complex amount in extra aqueous phase of interfacial polymerization could be directly detected by BCA assay and thus the protein loading amount can be calculated. Meanwhile, to further enhance the membrane water permeability, more AqpZ complex should be loaded into the barrier layer of the composite membrane. That is, in the interfacial polymerization membrane fabrication, specific binding (covalent conjugation) can be introduced between AqpZ/BP-1 complex and the surface, rather than non-specific binding. Consequently, peptide and the substrate need to be modified to functional groups accordingly.

In chapter 3, similar to chapter 2, to further improve the water permeability, improve the click efficiency might be one solution. In order to determine the click efficiency, the AqpZ complex click amount needs to be quantified. Fluorescein labeling might be a feasible method to quantify the protein click amount. Same as chapter 3, AqpZ could be labeled by FITC first and then perform the click conjugation between the protein complex and the polymeric substrate.

By testing the resulting click membrane and comparing the fluorescence signal with standard samples, the protein click amount could be calculated. Secondly, according to the preliminary desalination result of the click AqpZ-PSU membrane, after conjugation, the remaining open pores need be sealed to prevent ion leakage. This suggests that a dense barrier layer is required to cover the open pores area and block the ion leakage.

Intriguingly, bring the two methods together, here comes a new model of fabricating biomimetic desalination membranes—using click reaction to conjugate the AqpZ complex as the ultra high water permeable unit onto the functional polymeric substrate and sealing open pores by interfacial polymerization method to further increase the salt rejection. Similar to the work in Chapter 3, peptide and polymeric substrate could be modified with alkynyl and azide group, respectively, to perform the click reaction in the purpose of increasing the loading amount of AqpZ complex on the substrate. Interfacial polymerization reaction can be conducted afterwards. And proper reaction conditions of interfacial polymerization to fabricate the thin polyamide barrier layer require to be investigated.

References:

1. Shannon, M.A., et al., *Science and technology for water purification in the coming decades.* Nature, 2008. **452**(7185): p. 301-310.

2. Gleick, P.H., *Water resources.* Encyclopedia of climate and weather, 1996. **2**: p. 817-823.

3. UniCeF, *Progress on drinking water and sanitation: Special focus on sanitation*, in *Progress on drinking water and sanitation: special focus on sanitation*. 2008, WHO/JMP.

4. Focazio, M.J., et al., *A national reconnaissance for pharmaceuticals and other organic wastewater contaminants in the United States—II) Untreated drinking water sources.* Science of the Total Environment, 2008. **402**(2): p. 201-216.

5. Johnson, D.B. and G. Gleick, *The World's Water 2006-2007: The Biennial Report on Freshwater Resources.* Environmental Practice, 2008. **10**(3): p. 129.

6. Garcí, L., *Renewable energy applications in desalination: state of the art.* Solar energy, 2003. **75**(5): p. 381-393.

7. Al-Shammiri, M. and M. Safar, *Multi-effect distillation plants: state of the art.* Desalination, 1999. **126**(1): p. 45-59.

8. Wade, N.M., *Technical and economic evaluation of distillation and reverse osmosis desalination processes.* Desalination, 1993. **93**(1): p. 343-363.

9. Van der Bruggen, B. and C. Vandecasteele, *Distillation vs. membrane filtration: overview of process evolutions in seawater desalination.* Desalination, 2002. **143**(3): p. 207-218.

10. Al-Wazzan, Y. and F. Al-Modaf, *Seawater desalination in Kuwait using multistage flash evaporation technology—historical overview.* Desalination, 2001. **134**(1): p. 257-267.

11. Amjad, Z., *Reverse osmosis: membrane technology, water chemistry & industrial*

applications. 1993: Chapman & Hall.

12. Malek, A., M. Hawlader, and J. Ho, *Design and economics of RO seawater desalination.* Desalination, 1996. **105**(3): p. 245-261.

13. Miller, J.E., *Review of water resources and desalination technologies.* Sandia National Labs Unlimited Release Report SAND-2003-0800, 2003.

14. Commission, C.C., *California coastal resource guide.* 2009.

15. Lee, K.P., T.C. Arnot, and D. Mattia, *A review of reverse osmosis membrane materials for desalination—Development to date and future potential.* Journal of Membrane Science, 2011. **370**(1): p. 1-22.

16. Li, D. and H. Wang, *Recent developments in reverse osmosis desalination membranes.* Journal of Materials Chemistry, 2010. **20**(22): p. 4551-4566.

17. Reid, C. and E. Breton, *Water and ion flow across cellulosic membranes.* Journal of Applied Polymer Science, 1959. **1**(2): p. 133-143.

18. Loeb, S. and S. Sourirajan, *High-flow semipermeable membranes for separation of water from saline solutions.* Adv Chem Ser, 1962. **38**(1): p. 117-132.

19. Joshi, S. and A. Rao, *Cellulose triacetate membranes for seawater desalination.* Desalination, 1984. **51**(3): p. 307-312.

20. Edgar, K.J., et al., *Advances in cellulose ester performance and application.* Progress in Polymer Science, 2001. **26**(9): p. 1605-1688.

21. Hoehn, H.H. and J.W. Richter, *Aromatic polyimide, polyester and polyamide separation membranes*. 1980, Google Patents.

22. Credali, L., G. Baruzzi, and V. Guidotti, *Reverse osmosis anisotropic membranes based on polypiperazine amides*. 1978, Google Patents.

23. Senoo, M., S. Hara, and S. Ozawa, *Permselective polymeric membrane prepared from polybenzimidazoles*. 1976, Google Patents.

24. Rozelle, L.T., *Development of new reverse osmosis membranes for desalination.* 1968.

25. Cadotte, J.E., *Reverse osmosis membrane*. 1977, Google Patents.

26. Kawaguchi, T., et al., *Amphoteric ion-permeable composite membrane*. 1982, Google Patents.

27. Eriksson, P., *Water and salt transport through two types of polyamide composite membranes.* Journal of Membrane Science, 1988. **36**: p. 297-313.

28. Cadotte, J.E., *Interfacially synthesized reverse osmosis membrane*. 1981, Google Patents.

29. Micsonai, A., et al., *Accurate secondary structure prediction and fold recognition for circular dichroism spectroscopy.* Proceedings of the National Academy of Sciences, 2015. **112**(24): p. E3095-E3103.

30. Beitz, E., *Aquaporins*. Vol. 190. 2008: Springer Science & Business Media.

31. de Groot, B.L. and H. Grubmüller, *Water permeation across biological membranes: mechanism and dynamics of aquaporin-1 and GlpF.* Science, 2001. **294**(5550): p. 2353-2357.

32. *Structure of Aquaporin Reveals Mechanism for Transport Selectivity.* PLoS Biology, 2003. **1**(3): p. e75.

33. Zeidel, M.L., et al., *Reconstitution of functional water channels in liposomes containing purified red cell CHIP28 protein.* Biochemistry, 1992. **31**(33): p. 7436-7440.

34. Alberts, B., *Molecular Biology of the Cell: Reference edition*. 2008: Garland Science.

35. Borgnia, M.J., et al., *Functional reconstitution and characterization of AqpZ, the E. coli water channel protein.* Journal of molecular biology, 1999. **291**(5): p. 1169-1179.

36. Zhao, Y., et al., *Effects of proteoliposome composition and draw solution types on*

separation performance of aquaporin-based proteoliposomes: implications for seawater desalination using aquaporin-based biomimetic membranes. Environmental science & technology, 2013. **47**(3): p. 1496-1503.

37. Choi, H.-J. and C.D. Montemagno, *Recent Progress in Advanced Nanobiological Materials for Energy and Environmental Applications.* Materials, 2013. **6**(12): p. 5821-5856.

38. Taubert, A., A. Napoli, and W. Meier, *Self-assembly of reactive amphiphilic block copolymers as mimetics for biological membranes.* Current opinion in chemical biology, 2004. **8**(6): p. 598-603.

39. Zhang, L. and A. Eisenberg, *Multiple morphologies of" crew-cut" aggregates of polystyrene-b-poly (acrylic acid) block copolymers.* Science, 1995. **268**(5218): p. 1728-1731.

40. Jenekhe, S.A. and X.L. Chen, *Self-assembled aggregates of rod-coil block copolymers and their solubilization and encapsulation of fullerenes.* Science, 1998. **279**(5358): p. 1903-1907.

41. Stoenescu, R., A. Graff, and W. Meier, *Asymmetric ABC‐Triblock Copolymer Membranes Induce a Directed Insertion of Membrane Proteins.* Macromolecular bioscience, 2004. **4**(10): p. 930-935.

42. Kumar, M., et al., *Highly permeable polymeric membranes based on the incorporation of the functional water channel protein Aquaporin Z.* Proceedings of the National Academy of Sciences, 2007. **104**(52): p. 20719-20724.

43. Tao, H., et al., *Engineered nanostructured [beta]-sheet peptides protect membrane proteins.* Nature methods, 2013. **10**(8): p. 759-761.

44. Xiong, H., et al., *Periodicity of polar and nonpolar amino acids is the major determinant of secondary structure in self-assembling oligomeric peptides.* Proceedings of the National

Academy of Sciences, 1995. **92**(14): p. 6349-6353.

45. Schulz, G.E., *β-barrel membrane proteins.* Current opinion in structural biology, 2000. **10**(4): p. 443-447.

46. McGregor, C.-L., et al., *Lipopeptide detergents designed for the structural study of membrane proteins.* Nature biotechnology, 2003. **21**(2): p. 171-176.

47. Doig, A., *A three stranded β-sheet peptide in aqueous solution containing N-methyl amino acids to prevent aggregation.* Chemical Communications, 1997(22): p. 2153-2154.

48. Li, X., et al., *Preparation of supported lipid membranes for aquaporin Z incorporation.* Colloids and Surfaces B: Biointerfaces, 2012. **94**: p. 333-340.

49. Wang, H., et al., *Preparation and characterization of pore-suspending biomimetic membranes embedded with Aquaporin Z on carboxylated polyethylene glycol polymer cushion.* Soft Matter, 2011. **7**(16): p. 7274-7280.

50. Wang, M., et al., *Layer-by-Layer Assembly of Aquaporin Z-Incorporated Biomimetic Membranes for Water Purification.* Environmental science & technology, 2015. **49**(6): p. 3761-3768.

51. Wang, H., et al., *Highly Permeable and Selective Pore‐Spanning Biomimetic Membrane Embedded with Aquaporin Z.* Small, 2012. **8**(8): p. 1185-1190.

52. Duong, P.H., et al., *Planar biomimetic aquaporin-incorporated triblock copolymer membranes on porous alumina supports for nanofiltration.* Journal of Membrane Science, 2012. **409**: p. 34-43.

53. Zhong, P.S., et al., *Aquaporin-embedded biomimetic membranes for nanofiltration.* Journal of Membrane Science, 2012. **407**: p. 27-33.

54. Zhao, Y., et al., *Synthesis of robust and high-performance aquaporin-based biomimetic membranes by interfacial polymerization-membrane preparation and RO performance characterization.* Journal of Membrane Science, 2012. **423**: p. 422-428.

55. Li, X., et al., *Preparation of high performance nanofiltration (NF) membranes incorporated with aquaporin Z.* Journal of Membrane Science, 2014. **450**: p. 181-188.

56. Sun, G., et al., *Stabilization and immobilization of aquaporin reconstituted lipid vesicles for water purification.* Colloids and Surfaces B: Biointerfaces, 2013. **102**: p. 466-471.

57. Sun, G., et al., *A layer-by-layer self-assembly approach to developing an aquaporin-embedded mixed matrix membrane.* RSC Advances, 2013. **3**(2): p. 473-481.

58. Sun, G., et al., *Highly permeable aquaporin-embedded biomimetic membranes featuring a magnetic-aided approach.* RSC Advances, 2013. **3**(24): p. 9178-9184.

59. Wang, H.L., et al., *Mechanically robust and highly permeable AquaporinZ biomimetic membranes.* Journal of Membrane Science, 2013. **434**: p. 130-136.

60. Xie, W., et al., *An aquaporin-based vesicle-embedded polymeric membrane for low energy water filtration.* Journal of Materials Chemistry A, 2013. **1**(26): p. 7592-7600.

61. Lahann, J., *Click chemistry for biotechnology and materials science*. 2009: Wiley Online Library.

62. de Groot, B.L. and H. Grubmüller, *The dynamics and energetics of water permeation and proton exclusion in aquaporins.* Current opinion in structural biology, 2005. **15**(2): p. 176-183.

63. Zimmermann, R., *Condensation Polymers: By Interfacial and Solution Methods. Von PW Morgan. John Wiley & Sons, New York London ‐ Sydney 1965. 1. Aufl., XVIII, 561 S., zahlr. Abb., mehrere Tab., geb.£ 9.10.–*. Angewandte Chemie, 1966. **78**(16): p. 787-787.

64. Tewari, P.K., *Nanocomposite Membrane Technology: Fundamentals and Applications*. 2016: Taylor & Francis.

65. Hilal, N., A.F. Ismail, and C. Wright, *Membrane Fabrication*. 2015: CRC Press.

66. Carpino, L.A. and G.Y. Han, *9-Fluorenylmethoxycarbonyl amino-protecting group.* The Journal of Organic Chemistry, 1972. **37**(22): p. 3404-3409.

67. Merrifield, R.B., *Solid phase peptide synthesis. I. The synthesis of a tetrapeptide.* Journal of the American Chemical Society, 1963. **85**(14): p. 2149-2154.

68. Ghosh, A.K., et al., *Impacts of reaction and curing conditions on polyamide composite reverse osmosis membrane properties.* Journal of Membrane Science, 2008. **311**(1): p. 34-45.

69. Wijmans, J. and R. Baker, *The solution-diffusion model: a review.* Journal of membrane science, 1995. **107**(1): p. 1-21.

70. Gordon, D.J., K.L. Sciarretta, and S.C. Meredith, *Inhibition of β-amyloid (40) fibrillogenesis and disassembly of β-amyloid (40) fibrils by short β-amyloid congeners containing N-methyl amino acids at alternate residues.* Biochemistry, 2001. **40**(28): p. 8237-8245.

71. Zhang, S., et al., *Poly-N-methylated α-peptides: synthesis and X-ray structure determination of β-strand forming foldamers.* Chemical Communications, 2006(5): p. 497-499.

72. Chen, Y.-H., J.T. Yang, and K.H. Chau, *Determination of the helix and β form of proteins in aqueous solution by circular dichroism.* Biochemistry, 1974. **13**(16): p. 3350-3359.

73. Porter, M.C., *Handbook of industrial membrane technology.* 1989.

74. Morgan, P. and S. Kwolek, *Interfacial polycondensation. 2. Fundamentals of polymer formation at liquid interfaces.* Journal of Polymer Science, 1959. **40**(137): p. 299-327.

75. Freger, V., *Kinetics of film formation by interfacial polycondensation.* Langmuir, 2005.

21(5): p. 1884-1894.

76. Kuehne, M.A., et al., *Flux enhancement in TFC RO membranes.* Environmental progress, 2001. **20**(1): p. 23-26.

77. Tomaschke, J.E., *Interfacially synthesized reverse osmosis membrane containing an amine salt and processes for preparing the same*. 1990, Google Patents.

78. Kim, S.H., S.-Y. Kwak, and T. Suzuki, *Positron annihilation spectroscopic evidence to demonstrate the flux-enhancement mechanism in morphology-controlled thin-film-composite (TFC) membrane.* Environmental science & technology, 2005. **39**(6): p. 1764-1770.

79. Ghosh, A.K. and E.M. Hoek, *Impacts of support membrane structure and chemistry on polyamide–polysulfone interfacial composite membranes.* Journal of Membrane Science, 2009. **336**(1): p. 140-148.

80. Kolb, H.C., M. Finn, and K.B. Sharpless, *Click chemistry: diverse chemical function from a few good reactions.* Angewandte Chemie International Edition, 2001. **40**(11): p. 2004-2021.

81. Liang, L. and D. Astruc, *The copper (I)-catalyzed alkyne-azide cycloaddition (CuAAC)"click" reaction and its applications. An overview.* Coordination Chemistry Reviews, 2011. **255**(23): p. 2933-2945.

82. Liu, F., et al., *Diels–Alder reactivities of strained and unstrained cycloalkenes with normal and inverse-electron-demand dienes: Activation barriers and distortion/interaction analysis.* Journal of the American Chemical Society, 2013. **135**(41): p. 15642-15649.

83. Lowe, A.B., *Thiol-ene "click" reactions and recent applications in polymer and materials synthesis.* Polymer Chemistry, 2010. **1**(1): p. 17-36.

84. Bräse, S., et al., *Organic azides: an exploding diversity of a unique class of compounds.* Angewandte Chemie International Edition, 2005. **44**(33): p. 5188-5240.

85. Hong, V., et al., *Analysis and Optimization of Copper‐Catalyzed Azide–Alkyne Cycloaddition for Bioconjugation.* Angewandte Chemie International Edition, 2009. **48**(52): p. 9879-9883.

86. Dirks, A.T., et al., *Preparation of biohybrid amphiphiles via the copper catalysed Huisgen [3+ 2] dipolar cycloaddition reaction.* Chemical communications, 2005(33): p. 4172-4174.

87. Gopi, H., et al., *Structural determinants for affinity enhancement of a dual antagonist peptide entry inhibitor of human immunodeficiency virus type-1.* Journal of medicinal chemistry, 2008. **51**(9): p. 2638-2647.

88. Van de Witte, P., et al., *Phase separation processes in polymer solutions in relation to membrane formation.* Journal of Membrane Science, 1996. **117**(1): p. 1-31.

89. Avram, E., et al., *Polymers with pendant functional group. III. Polysulfones containing viologen group.* Journal of Macromolecular Science, Part A: Pure and Applied Chemistry, 1997. **34**(9): p. 1701-1714.

90. Yilmaz, G., et al., *Modification of polysulfones by click chemistry: amphiphilic graft copolymers and their protein adsorption and cell adhesion properties.* Journal of Polymer Science Part A: Polymer Chemistry, 2011. **49**(1): p. 110-117.

91. Meng, J.-Q., et al., *Synthesis of antifouling nanoporous membranes having tunable nanopores via click chemistry.* Journal of Membrane Science, 2012. **401**: p. 109-117.

92. Park, J.Y., et al., *Polysulfone-graft-poly (ethylene glycol) graft copolymers for surface modification of polysulfone membranes.* Biomaterials, 2006. **27**(6): p. 856-865.

93. Nakamoto, K., *Infrared and Raman spectra of inorganic and coordination compounds*. 1986: Wiley Online Library.

94. White, M.A., et al., *Toward the syntheses of universal ligands for metal oxide surfaces: controlling surface functionality through click chemistry.* Journal of the American Chemical Society, 2006. **128**(35): p. 11356-11357.

95. Billes, F., H. Endredi, and G. Keresztury, *Vibrational spectroscopy of triazoles and tetrazole.* Journal of Molecular Structure: THEOCHEM, 2000. **530**(1): p. 183-200.

96. Mirabella, F.M., *Internal reflection spectroscopy: Theory and applications*. Vol. 15. 1992: CRC Press.

97. Wagner, C.D. and G.E. Muilenberg, *Handbook of x-ray photoelectron spectroscopy: a reference book of standard data for use in x-ray photoelectron spectroscopy*. 1979: Physical Electronics Division, Perkin-Elmer Corp.

98. Gniewek, A., et al., *Pd-PVP colloid as catalyst for Heck and carbonylation reactions: TEM and XPS studies.* Journal of Catalysis, 2005. **229**(2): p. 332-343.

99. Xiang, T., et al., *Covalent deposition of zwitterionic polymer and citric acid by click chemistry-enabled layer-by-layer assembly for improving the blood compatibility of polysulfone membrane.* Langmuir, 2014. **30**(18): p. 5115-5125.

100. Ciampi, S., et al., *Functionalization of acetylene-terminated monolayers on Si (100) surfaces: a click chemistry approach.* Langmuir, 2007. **23**(18): p. 9320-9329.

101. Palacin, T., et al., *Efficient functionalization of carbon nanotubes with porphyrin dendrons via click chemistry.* Journal of the American Chemical Society, 2009. **131**(42): p. 15394-15402.

102. Wu, P., P. Hogrebe, and D.W. Grainger, *DNA and protein microarray printing on silicon nitride waveguide surfaces.* Biosensors and Bioelectronics, 2006. **21**(7): p. 1252-1263.

103. Ward, B., J.A. Notte, and N. Economou, *Helium ion microscope: A new tool for*

nanoscale microscopy and metrology. Journal of Vacuum Science & Technology B, 2006. **24**(6): p. 2871-2874.

104. Fox, D., et al., *Helium ion microscopy of graphene: beam damage, image quality and edge contrast.* Nanotechnology, 2013. **24**(33): p. 335702.

105. Ringler, P., et al., *Structure of the water channel AqpZ from Escherichia coli revealed by electron crystallography.* Journal of molecular biology, 1999. **291**(5): p. 1181-1190.

106. Savage, D.F., et al., *Architecture and selectivity in aquaporins: 2.5 Å X-ray structure of aquaporin Z.* PLoS Biol, 2003. **1**(3): p. E72.

107. Smith, P.K., et al., *Measurement of protein using bicinchoninic acid.* Analytical biochemistry, 1985. **150**(1): p. 76-85.